Pure lattice gauge theory in intermediate volumes. I

Bernd A. Berg
Department of Physics and Supercomputer Computations Research Institute, The Florida State University, Tallahassee, Florida 32306

Alain H. Billoire*
Supercomputer Computations Research Institute, The Florida State University, Tallahassee, Florida 32306
(Received 8 December 1988)

We investigate numerically the mass spectrum, string tension, deconfinement temperature, and lattice β function for pure SU(2) lattice gauge theory. Our data cover medium-sized volumes. Finite-size-scaling concepts are emphasized.

I. INTRODUCTION

Finite-size scaling[1,2] is a well-known concept in statistical mechanics and has also been formulated for quantum field theories.[3] One aim of our studies[4,5] is to demonstrate its usefulness for numerical investigations of lattice gauge theories. This paper gives a detailed presentation of the concepts underlying our investigation and our complete SU(2) Monte Carlo (MC) data. Compared to Refs. 4 and 5, the statistics have been extended considerably. Our data cover medium-sized volumes. This allows comparisons with recent analytical results.[6-8] Paper II of this series[9] collects exploratory SU(3) MC results.

We find that finite-size (Fisher) scaling turns also out to be a powerful tool for analyzing the MC data. Just by plotting results in a variable

$$z=\frac{L}{\xi} \tag{1.1}$$

one gains a lot of information. Here L is a length that characterizes the finite size of the system and ξ is a correlation length. In principle, any inverse mass qualifies as a correlation length in order to define a z variable. In what follows, if not noted otherwise, we mean by correlation length the inverse-mass gap $\xi=m^{-1}$, defined as the lightest mass state in the spectrum by the large distance falloff of a two-point function. The spin parity of this lightest state may change when lattice size and coupling constant are varied.

A (unfortunate) tendency in lattice gauge theory is to replace first principles by heuristic, "phenomenological" pictures. This ignores the original goal of lattice-gauge-theory simulations: namely, to replace heuristic QCD approaches by calculations from first principles. Understanding non-Abelian gauge theories (QCD without quarks) is a relevant step in this direction. In its lattice framework non-Abelian gauge theory constitutes a challenging problem of four-dimensional statistical mechanics. It is a regularization of Yang-Mills theory, defined by the Euclidean action

$$\begin{aligned} S&=\tfrac{1}{2}\int d^4x\ \mathrm{Tr}(F_{\mu\nu}F_{\mu\nu})\ , \\ F_{\mu\nu}&=\partial_\mu A_\nu-\partial_\nu A_\mu+ig[A_\mu,A_\nu]\ , \end{aligned} \tag{1.2}$$

where the gauge fields A_μ are Hermitian $N\times N$ matrices that belong to the SU(N) Lie algebra. The final aim is to remove the regularization and to obtain reliable results for the infinite-volume continuum theory.

Two problems emerge for results from finite lattices: namely, scaling violations and finite-lattice-size effects. (Definitions are given in the next section.) These two problems overlap. Using finite-size-scaling theory they may be disentangled. The situation is illustrated in Fig. 1. With $1/\xi$ (lattice spacing $a=1$) the ordinate represents a measure for the inverse ultraviolet cutoff, and the abscissa gives with $z=L/\xi$ a measure for the *physical size* of the system. In this paper the term *volume* is used with respect to the physical (and not the lattice) size. In principle we may reach the infinite-volume continuum limit along any line that approaches $1/\xi\to 0$ for $z\to\infty$. But our approach is to control scaling violations first, in the limit

$$\text{cutoff}\ \frac{1}{\xi}\to 0\ \text{ with } z=\frac{L}{\xi}=\text{const}\ . \tag{1.3}$$

The result of this *finite-volume continuum limit* is Yang-Mills theory in a continuous torus. The advantage is that this limit can be accurately controlled in many cases of interest. Repeating (1.3) for larger and larger z values, one approaches the infinite-volume continuum limit. In case of the glueball spectrum, the finite-volume corrections are quantitatively controlled by Lüscher's[10] equation

$$\begin{aligned} m(\infty)-m(z)=m(z)c_0\exp\left[-\frac{\sqrt{3}}{2}z\right] \\ +\text{higher orders in } z\ , \\ z\to\infty,\quad c_0>0\ . \end{aligned} \tag{1.4}$$

For arbitrary massive field theories this equation can be

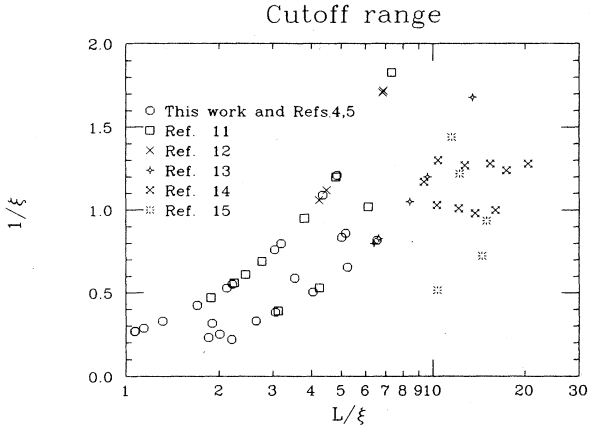

FIG. 1. Cutoff range where MC data are taken. $1/\xi \to 0$ is a measure for the ultraviolet cutoff and $L/\xi \to \infty$ for the finite size of the volume. No error bars are given as we are merely interested in a qualitative overview. Our data from $L_t L^2 L_z$, $L_t < L \ll L_z$ lattices are not included in this figure.

proven to all orders of perturbation theory (c_0 is related to the three-meson coupling constant) and it is also conjectured to hold for non-Abelian gauge theories. Like the Callan-Symanzik equation it is a structural equation that is supposed to be valid beyond perturbation theory. Typically, our numerical results are reliable in the range up to (and somewhat beyond) $z \approx 5$. Clearly, $\exp[-(\sqrt{3}/2)5] \approx 0.013$ is already a small number. Unfortunately, it is *a priori* not known how large z has to be for Eq. (1.4) to hold. But let us remark that small- and medium-sized volumes in the sense of our paper are not identical with small- and medium-sized lattices. The limit (1.3) requires infinite lattices, whatever the value of z is; fortunately our data show that for small z the limit $1/\xi \to 0$ is already well approached on rather small lattices. Figure 1 compares the range where our data are taken with other investigations.[11–15] The variable z is plotted on a log scale, as the (asymptotic) large-z corrections are exponentially small, whereas the ultraviolet corrections are of order $1/\xi$. We note that the trend of most investigations (with notable recent exceptions[15]) is to go to rather large volumes without keeping $1/\xi$ small, whereas we (and Ref. 11) achieve smaller $1/\xi$ values at the price of staying at smaller volumes.

Yang-Mills theory in a finite continuous torus was first investigated by 't Hooft.[16] Results for the lattice theory can be found in Refs. 17–19. He noticed that, for each of the "spacelike" directions, the Hamiltonian commutes with a group of global Z_N transformations related to the center of the SU(N) gauge group. These transformations are called "central conjugations." Operators that transform nontrivially under the Z_N transformations carry 't Hooft electric flux. The quantum numbers of electric flux are

$$\mathbf{q} = (q_1, q_2, q_3) \quad \text{with } q_i \in Z_N \ , \tag{1.5}$$

where the index i corresponds to the spacelike directions of the torus. Classical minima of the action that are not pure gauge configurations exist on the torus. They are called "torons."[19] A finite subset of the toron manifold, the so-called singular or "quantum-mechanically" stable torons, are of fundamental importance.

In his pioneering work[20] Lüscher pointed out that small volumes allow to compute the energy levels perturbatively using a low-energy effective Hamiltonian for the SU(N) Yang-Mills theory (1.2). In subsequent papers the SU(2) (Ref. 21) and SU(3) (Ref. 22) glueball spectrum was investigated for Lüscher's one-loop effective Hamiltonian. Rayleigh-Ritz variational calculations turned out to be an effective method. Lüscher and Münster chose harmonic-oscillator-type trial wave functions

$$\psi(c) = Q(c) \exp(-\tfrac{1}{2}\omega c_k^a c_k^a) \ ,$$

which are rapidly decaying in the constant gauge potentials c_k^a [$k = 1,2,3$ are space indices, $a = 1,2,3$ are SU(2)-color indices, and Q is a polynomial in the c_k^a]. This choice was motivated by the fact that the eigenfunctions of the lowest-order effective Hamiltonian H_0' are analytic and rapidly decaying. For the variational calculation the oscillator frequency ω can be optimized. Clearly, all such trial wave functions are concentrated on one of the toron vacuum sectors and, in this way, their boundary conditions reflect the perturbative nature of the approach. In particular, the 't Hooft electric flux stays zero to all orders of the perturbative expansion.

The first attempt to include nonperturbative physics into Lüscher's small-volume expansion was made in the semiclassical approximation by van Baal and Koller.[23] They named "tunneling transition" a rapid increase of the 't Hooft electric flux due to tunneling between the N^3 toron sectors. Semiclassical methods turned out to be sufficiently accurate to indicate the approximate location of the tunneling transition (consistent with independent numerical work[4,5,24]) to be at $z \approx 1$, and this is where the perturbative approach[21,22] breaks down. However, in a very interesting recent contribution Koller and van Baal[6,7] found out that nonperturbative physics can be obtained from Lüscher's effective Hamiltonian by imposing appropriate nonperturbative boundary conditions to the Rayleigh-Ritz trial wave functions. In Ref. 7 this is named the "*adiabatic approximation*." Although the systematics of corrections to the calculation by Koller and van Baal is not understood, our MC results give evidence that their approach is valid up to $z \approx 5$. A detailed comparison of numerical and analytical results is carried out in this paper. The range up to $z \approx 1$ (this means before the tunneling transition) will be called small volume and the range between $z \approx 1$ and $z \approx 5$ (this means after the tunneling transition) defines the *intermediate volume*. Large volumes are in the range above $z \approx 5$. The reason for the further division between intermediate and large volumes (which may not be sharp) is that various results[7,25,15,26] [note that the $m(T_2^+)$ result of Ref. 7 is corrected Ref. 25] support the opinion that substantial changes in physics still take place in the volume range around (or even above) $z \approx 5$.

Let us conclude the Introduction with a short outline of the paper. Section II summarizes the basic concepts

and our notation. Subsection II A discusses the transfer matrix and correlation functions, II B the string tension definitions of Wilson, Polyakov, and 't Hooft, II C our trial operators and the mass spectrum, II D finite-size scaling and finite-size problems, II E the deconfinement phase transition, II F the the lattice β function, and II G Monte Carlo data and error estimates. Section III presents our numerical results. Subsection III A discusses the raw data, III B the string tension and lattice β function, III C the glueball masses and large volume extrapolations, III D addresses the question: glueballs or flux states? Section III E considers deconfinement, tunneling, and string formation. Summary and conclusions are given in Sec. IV.

II. SU(N) LATTICE GAUGE THEORY AND MONTE CARLO SIMULATIONS

We assume that the reader is familiar with lattice gauge theories. Reviews are presented elsewhere (see, for instance, Ref. 27). The aim of this section is to keep our paper self-contained and to emphasize aspects that are relevant for (our) numerical investigations.

For SU(N) lattice gauge theory (without quarks) one has to calculate expectation values $\langle\cdot\rangle$ of gauge-invariant operators with respect to the partition function

$$Z=\int\prod_l dU(l)\exp(-\beta S)\ , \tag{2.1a}$$

where in our investigation

$$S=\frac{1}{N}\left[\sum_p \mathrm{Re\,Tr}[1-U(p)]\right] \tag{2.1b}$$

is the standard Wilson[28] action. The product in Eq. (2.1a) is over all links l of a four-dimensional hypercubic lattice with lattice spacing a and $U(l)\in\mathrm{SU}(N)$. For each plaquette p, $U(p)$ is the ordered product of the four link matrices surrounding the plaquette and dU is the SU(N) Hurwitz measure. β is related to the coupling constant by

$$g^2=\frac{2N}{\beta}\ . \tag{2.1c}$$

In this paper we restrict our discussion to lattices with periodic boundary conditions. Periodic boundary conditions avoid spurious ultraviolet effects, which would be introduced by sharp boundaries. Our lattices have size

$$L_t L^2 L_z \quad \text{with } L_t\le L\le L_z\ . \tag{2.2}$$

If $L_z\gg L$ we use the notation "$L_t L^2\infty$ *lattices.*" In particular we are interested in the cases

$$L_t=L\ll L_z \tag{2.3a}$$

(often called $L^3\infty$ geometry in what follows)

and

$$L_t<L=L_z\ . \tag{2.3b}$$

Let us now consider (2.3a) and assume that we have carried out the limit $L\to\infty$. Then the renormalization-group equation

$$\left[-a\frac{\partial}{\partial a}+\beta_L(g)\frac{\partial}{\partial g}\right]m(g,a)=0$$

holds for any mass m expressed in physical units, and defines the lattice (subscript L) β function $\beta_L(g)$. A well-known[29] two-loop calculation gives the two universal expansion coefficients of the β function:

$$\beta_L(g)=-\beta_0 g^3-\beta_1 g^5+O_L(g^7)$$

$$\text{with } \beta_0=\frac{11}{3}\frac{N}{16\pi^2} \text{ and } \beta_1=\frac{34}{3}\left[\frac{N}{16\pi^2}\right]^2 .$$

The renormalization-group equation is easily integrated and predicts quantitatively how the continuum limit is approached: namely,

$$m=\mathrm{const}_m\Lambda_L[1+F_L^m(g^2)]\ , \tag{2.4a}$$

where the lattice scale Λ_L is defined by

$$\Lambda_L=\Lambda_L(g)$$

$$=a^{-1}(\beta_0 g^2)^{\alpha}\exp\left[-\frac{1}{2\beta_0 g^2}\right],\quad \alpha=-\frac{\beta_1}{2\beta_0^2}\ . \tag{2.4b}$$

If a value g_0 exists such that $m=\mathrm{const}_m\Lambda_L$ holds for $g^2\le g_0^2$ within some required numerical precision (e.g., 10%) we call this behavior *asymptotic scaling.* There are order-g^2 corrections to asymptotic scaling. The function $F_L^m(g^2)$ measures the deviations from asymptotic scaling and is related to the $O_L(g^7)$ corrections of the lattice β function. Its perturbative expansion is

$$F_L^m(g^2)=\epsilon_1 g^2+\epsilon_2 g^4+\cdots\ .$$

Here ϵ_1 is determined by the nonuniversal three-loop term in $\beta_L(g^2)$, etc. Furthermore, F_L^m has exponentially small nonperturbative contributions, i.e., contributions of order $a^2\ln a$. The nonperturbative contributions may vary for different masses.

According to Symanzik[30] the perturbative corrections to asymptotic scaling are expected to drop out for mass ratios and one finds

$$\frac{m_1}{m_2}=\mathrm{const}_{12}+O(a^2\ln a)\ . \tag{2.5}$$

If $m_1/m_2=\mathrm{const}_{12}$ is true within the requested numerical precision we call this *scaling (in general).* The approach to scaling is supposed to be faster than to asymptotic scaling because of Eq. (2.4b) $a\sim\Lambda_L^{-1}\exp[-1/(2\beta_0 g^2)]$ for $g^2\to 0$

Let us consider the geometry (2.3b). In the limit $L\to\infty$, one encounters the deconfining phase transition[31,32] at $g_c=g_c(L_t)$. In the deconfined phase the global Z_N symmetry under the center of the gauge group is broken, whereas in the confinement regime this symmetry is preserved. This defines the deconfining temperature $T_c=T_c(g_c)=1/L_t(g_c)$. The deconfining temperature is a physical quantity with the dimension of a mass, it is expected to behave like the other physical masses

$$T_c=\mathrm{const}_T\Lambda_L(g_c)[1+F_L^T(g_c^2)]\ . \tag{2.4c}$$

We try to carry out the limit (1.3) to match on analytical calculations which exist for small and intermediate volumes. The analytic calculations use dimensional regularization and the natural scale is $\Lambda_{\overline{\rm MS}}$, where MS denotes the minimal subtraction scheme. The well-known (see, for instance, Refs. 21 and 33) relationship

$$\Lambda_{\overline{\rm MS}}=7.5\ \Lambda_L \tag{2.6}$$

establishes the connection with lattice calculations. In the actually used approximations, finite lattice in case of MC investigations and one-loop computation in case of the adiabatic approximation, we have higher-order corrections. So far no attempt has been made to calculate these corrections systematically and the comparison on the Λ-scale level cannot be expected to be very accurate. For mass ratios the situation should be better, as corrections to lattice results are supposed to come from scaling (not asymptotic scaling) violations only. The situation for the adiabatic approximation is different and perturbative corrections are possible for mass ratios. Nevertheless we think that mass ratios are better behaved than results in Λ units.

A. Transfer matrix and correlation functions

We consider the general geometry (2.2). Let

$$\mathcal{T}=\mathcal{T}(L_t,L) \tag{2.7}$$

be the transfer matrix in L_z direction. Obviously, the transfer matrix does not depend on the L_z extension of the lattice. For the Wilson action (2.1b) the transfer matrix is well known to be positive definite.[34] We define eigenstates and eigenvalues by means of

$$\mathcal{T}|n\rangle=\lambda_n|n\rangle \quad \text{with } \lambda_n=e^{-m_n},\ \ \lambda_{n+1}\le\lambda_n,\ \ n\ge 0\ . \tag{2.8}$$

The vacuum state is denoted by $|0\rangle$ and we adopt the normalization $\lambda_0=1$ (equivalently $m_0=0$). As a consequence of the Perron-Frobenius theorem,[35] the vacuum is unique for finite systems. Furthermore, the eigenstates are chosen to be orthonormal $\langle n|k\rangle=\delta_{nk}$.

With m_n we label not only masses but also momentum. This may be expressed by the correspondence (for $n\ge 1$)

$$n\equiv(i,\mathbf{p}),\ \ i\ge 1,\ \ p_1=\frac{2\pi k_1}{L_t},\ \ p_j=\frac{2\pi k_j}{L}\ \ (j=2,3)\ .$$

In the infinite-volume continuum limit relativistic invariance implies $m_{(i,\mathbf{p})}=[m_{(i,0)}+\mathbf{p}^2]^{1/2}$. In the Hilbert space sector which is obtained by applying flux-zero, gauge-invariant operators $\mathcal{O}_n$ to the vacuum $|n\rangle=\mathcal{O}_n|0\rangle$, the states of non-Abelian gauge theories are called glueballs.[36]

Consider the expectation value of a gauge-invariant operator $\mathcal{O}$ that is local in time. On a lattice with finite L_z we have

$$Z=Z(L_t,L,L_z)=\mathrm{Tr}(\mathcal{T}^{L_z})=\sum_n e^{-m_nL_z}$$
$$=1+O(e^{-m_1L_z}) \tag{2.9a}$$

and

$$\langle\mathcal{O}\rangle=Z^{-1}\sum_n\langle n|\mathcal{O}|n\rangle e^{-m_nL_z} \tag{2.9b}$$

holds. Clearly, L_z^{-1} plays the role of a temperature. It is analog to 't Hooft's[16] temperature definition for a continuous L^3L_z, $L\ll L_z$ volume. As there is no preferred time direction in Euclidean space, we are now at a possible point of confusion. In the context of the analytical work (Refs. 16, 20, 7, and others) our L_z direction is chosen as time direction [obtained from our notation by the cyclic permutation $(t,x,y,z)\to(x,y,z,t)$]. This makes the definition of "electric" flux natural, its components are spacelike and obtained from correlations of Polyakov loops in time direction. However, a problem arises when the thus defined "spacelike" volume is rather small in appropriate physical units. In numerical studies of finite-temperature effects and, in particular, of the deconfining phase transition[32] the smallest lattice extension is identified with the time direction (L_tL^3 lattices with $L_t<L$) and related to the physical temperature. As part of our investigations are devoted to a study of the deconfining phase transition, we decided to stay as close as possible to the latter notation and to extend it to the case of L^3L_z ($L<L_z$) lattices by identifying one of the three L^3 directions with the time, hence our notation of $L_tL^2\infty$ lattices. In the limit $L\to\infty$ we get the standard geometry of numerical deconfinement investigations. Physically, this choice of the time direction is related to interpreting Polyakov loop correlation functions as quark-antiquark potential (see next section), then the time direction is the one in which the loop closes. For practical purposes our generalization makes sense, we shall see in Sec. II E that a finite-size scaling comparison of systems as small in L as 4×4^264 vs 4×6^264 already allows to study relevant finite-temperature effects. To distinguish between the two temperature definitions we define

$$T_b=L_z^{-1} \tag{2.10}$$

and call T_b (lattice) *box temperature,* because it has the interpretation of the temperature of the L_tL^2 box. (The name for this temperature is of course rather arbitrary, here we stay consistent with our first investigations.[24]) The box temperature has to be distinguished from the *physical temperature* T_p defined by

$$T_p=L_t^{-1}\ . \tag{2.11}$$

For $L_z\to\infty$ and L_t,L fixed, the system approaches zero box temperature. This means

$$\langle\mathcal{O}\rangle=\langle0|\mathcal{O}|0\rangle,\ \ Z=1 \tag{2.12}$$

holds, where $|0\rangle=|0\rangle_{(L_t,L)}$ is the vacuum of the L_tL^2 "spacelike" box [for simplicity we shall suppress the subscript (L_t,L)]. $L_z<\infty$ implies finite box-temperature corrections which we discuss next.

To calculate the mass spectrum numerically, the standard method is to analyze correlation functions of gauge-invariant, Hermitian operators. Let us define

$$\mathrm{ch}_m(t_z)=e^{-mt_z}+e^{-m(L_z-t_z)} . \tag{2.13}$$

Connected correlation functions for the operator $\mathcal{O}$ are defined by

$$\begin{aligned} C_{\mathcal{O}}(t_z)&=\langle \mathcal{O}(0)\mathcal{O}(t_z)\rangle_c \\ &=\langle \mathcal{O}(0)\mathcal{O}(t_z)\rangle-\langle \mathcal{O}(0)\rangle\langle \mathcal{O}(t_z)\rangle , \end{aligned} \tag{2.14a}$$

where $t_z=0,1,2,\ldots,L_z-1$ is the separation in the z direction. The dependence on t_x,t_y,t_t (x,y,t direction) is chosen to be identical for $\mathcal{O}(0)$ and $\mathcal{O}(t_z)$ and therefore suppressed. Positivity of the transfer matrix implies $C_{\mathcal{O}}(t_z)>0$. The implicit equation

$$\frac{C_{\mathcal{O}}(t_z)}{C_{\mathcal{O}}(t_z-1)}=\frac{\mathrm{ch}_{m(t_z)}(t_z)}{\mathrm{ch}_{m(t_z)}(t_z-1)} \tag{2.14b}$$

defines $m(t_z)$, the *effective mass* at distance t_z. The equation

$$\mathcal{O}(0)|n\rangle=\sum_i c_i^n|i\rangle, \quad c_i^n \text{ real}, c_n^i=c_i^n \tag{2.15}$$

implies that correlation functions are given by

$$\begin{aligned} \langle \mathcal{O}(0)\mathcal{O}(t_z)\rangle&=Z^{-1}\mathrm{Tr}(\mathcal{O}\mathcal{T}^{t_z}\mathcal{O}\mathcal{T}^{L_z-t_z}) \\ &=Z^{-1}\sum_n \langle n|\mathcal{O}\mathcal{T}^{t_z}\mathcal{O}|n\rangle e^{-m_n(L_z-t_z)} \\ &=Z^{-1}\sum_n\sum_i (c_i^n)^2 e^{-m_i t_z}e^{-m_n(L_z-t_z)} . \end{aligned} \tag{2.16}$$

The connected part is

$$\begin{aligned} \langle \mathcal{O}(0)\mathcal{O}(t_z)\rangle_c&=a_0+\sum_{i\geq 1} a_i \mathrm{ch}_{m_i}(t_z) \\ &\quad+\sum_{i>n,n\geq 1} b_i^n \mathrm{ch}_{(m_i-m_n)}(t_z) \end{aligned} \tag{2.17}$$

with

$$a_0=Z^{-1}\sum_n (c_n^n)^2 e^{-m_n L_z}-\left[Z^{-1}\sum_n c_n^n e^{-m_n L_z}\right]^2 \geq 0 , \tag{2.18a}$$

$$a_i=Z^{-1}(c_0^i)^2, \quad i=1,2,\ldots, \tag{2.18b}$$

and

$$b_i^n=Z^{-1}(c_i^n)^2 e^{-m_n L_z} . \tag{2.18c}$$

We show in Appendix A that $a_0\geq 0$. For operators with

$$c_n^n=\langle n|\mathcal{O}|n\rangle=0 \quad \text{for } n=0,1,2,\ldots, \tag{2.19}$$

we have $a_0=0$. Otherwise a_0 will only approach $0=(c_0^0)^2-(c_0^0)^2$ in the limit $L_z\to\infty$. The last term in Eq. (2.17) can also contribute positive constant terms, if there exist states with $m_i=m_n$ and nonzero b_i^n. In addition, as we have no analytical control over the mass differences (m_i-m_n) in these b_i^n terms, the lowest mass which appears in a correlation function is likely not a mass but a mass difference. The finite-box temperature is thus shown to have two effects: (i) e^{-mt_z} becomes $\mathrm{ch}_m(t_z)$; (ii) new contributions (2.18a)–(2.18c) appear which may cause a spurious decrease of effective masses for large t_z. Although these contributions are exponentially small like $e^{-m_1 L_z}$ they do show up in our MC data. Presumably this happens due to a large number of contributing terms.

B. String tension of Wilson, Polyakov, and 't Hooft

In this subsection we introduce confinement concepts of Wilson,[28] Polyakov,[31] 't Hooft,[16] and their associated string tensions. A thorough treatment has been given in the article by Borgs and Seiler.[37]

For large distance R the continuum potential $V(R)$ between two infinitely heavy quarks ($q\bar{q}$) is of the form

$$V(R)=\kappa R+c_0+c_1 R^{-1}+O(R^{-2}) , \tag{2.20}$$

where κ is the string tension and the coefficient c_1 describes the Coulomb correction. String theory predicts[38] the coefficient of the R^{-1} correction to be

$$c_1=-\frac{\pi}{12} . \tag{2.21}$$

On the lattice, rectangular $R\times T$ Wilson[28] loops $\mathcal{W}(T,R)$ allow to define a lattice potential $V_{\mathrm{lat}}^W(R)$ which describes the total energy of two infinitely heavy quarks separated by a distance R. For T sufficiently large we have

$$W(T,R)=\langle \mathcal{W}(T,R)\rangle\sim\exp[-TV_{\mathrm{lat}}^W(R)] .$$

The relation between the continuum potential $V(R)$ and the lattice potential is

$$V_{\mathrm{lat}}^W(R)=V(R)+V_0 .$$

Here V_0 is the lattice-spacing-dependent self-energy of the infinitely heavy quark. The Wilson string tension κ_W is defined as

$$\kappa_W=\kappa_W^\infty=\lim_{R\to\infty}\lim_{T\to\infty}\lim_{L\to\infty}\frac{1}{R}V_{\mathrm{lat}}^W(R) , \tag{2.22}$$

where a $L_t=L=L_z$ lattice is assumed. Finite-size effects for the Wilson string tension are somewhat subtle to investigate, because not only the size of the lattice but also the sizes of the loops are involved.

Polyakov[31] loops $\mathcal{P}$ are Wilson lines which are closed (in L_t or L direction) by the periodic boundary conditions. They allow a variant definition of the string tension. Let us assume the $L_t L^2 L_z$ geometry (2.2) and close the Polyakov loop in L_t direction. The expectation value of the Polyakov loop is an order parameter with respect to the Z_N central conjugations. In the infinite-volume limit, this expectation value is related to the free energy F_q of a single static, infinitely heavy quark $\langle\mathcal{P}\rangle\sim\exp(-L_t F_q)$. Correlations of Polyakov loops therefore give the free energy of a static quark-antiquark potential $V_{\mathrm{lat}}^P(t_z)$ by means of

$$\begin{aligned} &\langle \mathcal{P}(0)\bar{\mathcal{P}}(t_z)\rangle \\ &\quad=\text{const}\times(e^{-L_t V_{\mathrm{lat}}^P(t_z)}+e^{-L_t V_{\mathrm{lat}}^P(L_z-t_z)}) . \end{aligned} \tag{2.23}$$

Here $\bar{\mathcal{P}}$ is in the conjugate representation [$\bar{\mathcal{P}}=\mathcal{P}$ for SU(2)] and the (t_t,t_x,t_y) dependence is as in Eq. (2.14a). The *Polyakov string tension* κ_P is defined by

$$\kappa_P=\kappa_P(L_t,L)=\lim_{t_z\to\infty}\lim_{L_z\to\infty}\frac{1}{t_z}V^P_{\rm lat}(t_z)\ . \tag{2.24}$$

For brevity we often denote κ_P just by κ in the forthcoming. Measuring correlations between zero-momentum Polyakov loops is an efficient way to extract κ directly, see Sec. II C.

't Hooft's[16] way of looking at the confinement problem consists of studying the free energy of an electric (or magnetic) flux tube impressed by "twisted" boundary conditions on a periodic continuous box. Mack and Petkova[17] introduced the equivalent concept of free energy of "vortices" in a "vortex container." Their vortices are the fluxons of 't Hooft. "Twist" on the lattice was extensively studied by Ref. 18. Assume we introduce a twist in L_t direction and let $E_1(L_t,L,L_z)$ be the difference in free energy as compared with the untwisted configuration. The 't Hooft string tension is defined by

$$\kappa_H=\kappa_H(L_t,L)=\lim_{L_z\to\infty}\frac{1}{L_z}E_1(L_t,L,L_z)\ . \tag{2.25}$$

[In some papers the name 't Hooft string tension is used for the Polyakov string tension on $L^3\infty$ lattices. This is natural when our L_z direction is identified with the time and one gets then $E_1=E_1(L_x,L_y,L_z)$; see our discussion in front of Eq. (2.10).] Rigorously[37] it has only been proven that

$$\kappa_W\geq\lim_{L_t\to\infty}\lim_{L\to\infty}\kappa_P(L_t,L)\quad\text{and}\quad\kappa_P(L_t,L)\geq\kappa_H(L_t,L)\ . \tag{2.26a}$$

This means confinement in the sense of 't Hooft implies confinement in the sense of Polyakov and Wilson. Within the validity of the strong-coupling expansion Münster[39] has shown that $\kappa_W=\lim_{L_t\to\infty}\lim_{L\to\infty}\kappa_H$ holds and this equality is conjectured to survive all the way to the continuum limit (i.e., for all β). As Polyakov loops project onto the electric flux one sector, equality

$$\kappa_P(L_t,L)=\kappa_H(L_t,L) \tag{2.26b}$$

is true to the extent that the Polyakov loops couple to the ground state in the flux one sector. In the forthcoming we always assume (2.26b) and calculate energies of flux states from correlations between Polyakov loops. In what follows we will call string tension the flux tube energy divided by its length

$$E_1=L_t\kappa\ , \tag{2.27}$$

although "string formation" is expected to take place only for large volumes. In case of the symmetric L^3L_z geometry the name electric flux (1.5) applies to all three "space" directions. For SU(2) the energy E_1 is associated with $\mathbf{q}=(1,0,0)$, (0,1,0), or (0,0,1). Energies corresponding to higher units of electric flux can be obtained from correlations of appropriate products of Polyakov loops (see next section). For SU(2) the energy E_2 is associated with two units of electric flux $\mathbf{q}=(1,1,0)$, (1,0,1), or (0,1,1) and energy E_3 corresponds to three units of electric flux $\mathbf{q}=(1,1,1)$.

In case of an asymmetric lattice $L_t<L<L_z$ it can be appropriate to consider L^2L_z as the spacelike box (correlations are still measured in L_z direction). In this situation we define for one unit of flux

$$E_t=L_t\kappa_t\quad\text{and}\quad E_s=L\kappa_s \tag{2.28}$$

to distinguish energies from loops closed in L_t or L direction, respectively.

At finite box-temperature flux states may contaminate vacuum results.[40] This becomes relevant on lattices where the 't Hooft electric flux is the smallest eigenvalue (above the vacuum) of the Euclidean Hamiltonian. For SU(N) and an L^3L_z lattice the leading contamination is [see Eqs. (2.9) for definitions]

$$\begin{aligned}Z\langle\mathcal{O}\rangle-\langle 0|\mathcal{O}|0\rangle=&3(N-1)[\langle E_1|\mathcal{O}|E_1\rangle e^{-E_1L_z}+\langle E_2|\mathcal{O}|E_2\rangle e^{-E_2L_z}]+(N-1)\langle E_3|\mathcal{O}|E_3\rangle e^{-E_3L_z}\\&+3(N-1)^2\langle 2E_1|\mathcal{O}|2E_1\rangle e^{-2E_tL_z}+\cdots\ .\end{aligned} \tag{2.29}$$

C. Trial operators and spectrum

Numerical investigations try to infer on the mass spectrum from correlation functions of trial operators. The central problem is to find good trial operators. The following two properties are needed: (i) The trial operator should have a large projection on the wave function of the investigated state; (ii) the trial operator should give a clear signal that allows to follow correlations up to large distances.

The states are classified according to the irreducible representations of the three-dimensional cubic group,[41] denoted by A_1, E, T_2, T_1, and A_2. The representations of the one-plaquette operator were given by Kogut, Sinclair, and Susskind,[42] and in Ref. 43 the irreducible representations of the cubic group were systematically constructed for all Wilson loops with a perimeter ≤ 8. Older MC investigations of the glueball spectrum mainly relied on such Wilson loops, for a review see Ref. 44. In the sense made precise in Ref. 43, the listed irreducible representations of the cubic group correspond, respectively, to spins 0, 2, 2, 1, and 3 in the continuum limit. With present-day simulation methods it seems rather hopeless to investigate states other than lowest-lying states above the vacuum.

The trial operators of this paper are Polyakov loops in

the fundamental as well as in the adjoint and higher representations. Most simulations were done in the $L^3\infty$ geometry. As discussed, correlations in the fundamental representation gives rise to the Polyakov–'t Hooft string tension. A numerical investigation was first carried out by Parisi, Petronzio, and Rapuano.[45]

In the adjoint representation Polyakov loops $\mathcal{A}$ couple to glueballs. The momentum zero loops are good trial operators for the A_1^+ and the E^+ state in medium-sized volumes. At large β the signal is improved by several orders of magnitude[4] as compared to the signal from correlations between Wilson-loop trial operators.[44] We conjecture that this fact is related to the different short-distance (spin-wave) behavior of (zero-momentum) Polyakov and Wilson loops: namely,

$$\sim t_z^{-1} \text{ (adjoint Polyakov loops)}$$

and (2.30)

$$\sim t_z^{-5} \text{ (Wilson loops)}, \quad \beta\to\infty \ .$$

Equation (2.30) means that for Wilson loops the signal disappears rapidly at large β. For $\beta\to 0$ the plaquette operator only couples to the lowest glueball state, whereas Polyakov loops fade away. In MC simulations adjoint Polyakov loops were first measured to investigate the adjoint string tension.[46]

Let $\mathcal{O}_i$ be a Polyakov loop, closed in direction i, $(i=t,x,y)$ of the $L_t L^2$ box. Zero-momentum operators are defined by summing over the transverse directions

$$\mathcal{O}_t(t_z)=\sum_{t_y,t_x}\mathcal{O}_t(t_x,t_y,t_z), \text{ etc} \ .$$

In the symmetric case ($L_t=L$) the following combinations project on the one-dimensional A_1^+ and the two-dimensional E^+ representations

$$\mathcal{O}_{A_1^+}(t_z)=\mathcal{O}^t(t_z)+\mathcal{O}^x(t_z)+\mathcal{O}^y(t_z) \ , \tag{2.31a}$$

$$\mathcal{O}_{E^+(1)}(t_z)=\mathcal{O}^t(t_z)-\mathcal{O}^x(t_z) \ , \tag{2.31b}$$

and

$$\mathcal{O}_{E^+(2)}(t_z)=\mathcal{O}^t(t_z)+\mathcal{O}^x(t_z)-2\mathcal{O}^y(t_z) \ . \tag{2.31c}$$

These combinations are of practical importance for glueballs. For Polyakov loops in the fundamental representation, electric flux conservation implies that the correlation function of two loops in different directions is zero. There is no point introducing A_1^+ and E^+ representations, we rather consider the single correlation function

$$C_{\mathcal{P}}(t_z)=\sum_i\langle\mathcal{P}_i(0)\mathcal{P}_i(t_z)\rangle \ ,$$

which gives the statistically most accurate results. As first emphasized in Ref. 47, through the projection effective energies $E_1(t_z)$, defined by (2.14b), are no longer spoiled by contributions from states with nonzero momenta and $E_1(t_z)$ converges rapidly with t_z. For SU(3) Ding[48] has directly compared E_1 results from fits of the potential $V_{\text{lat}}^P(t_z)$ versus those from direct zero-momentum correlations. As expected consistency is found and the latter approach improves the accuracy by a factor of approximately 4 (16 in computer time).

Our trial operators for two units of electric flux (energy E_2) are

$$\mathcal{P}_i^2(t_z)=\mathcal{P}_j(t_z)\mathcal{P}_k(t_z) \quad \text{with } i\neq j\neq k \ , \tag{2.32a}$$

and for three units of electric flux (energy E_3) it is

$$\mathcal{P}^3(t_z)=\mathcal{P}_1(t_z)\mathcal{P}_2(t_z)\mathcal{P}_3(t_z) \ . \tag{2.32b}$$

Definitions of E_2 and E_3 are given after Eq. (2.27).

For measurements of Polyakov loops we used the Dobrushin-Lanford-Ruelle (DLR) improvement scheme.[49,45] At intermediate and small β values this suppression of statistical noise turned out to be crucial. The improvement is achieved by integrating appropriate link variables with the Hurwitz measure. The SU(2) master formula

$$\frac{\int dU\, D_{ij}^J(U)e^{\beta\,\mathrm{Tr}(UV^\dagger)/2}}{\int dU\, e^{\beta\,\mathrm{Tr}(UV^\dagger)/2}}=\frac{I_{2J+1}(\lambda\beta)}{I_1(\lambda\beta)}D_{ij}^J(W)$$

$$\text{with } V=\lambda W, \quad W\in\mathrm{SU}(2), \quad \lambda \text{ real} \tag{2.33}$$

is easily proven using equations from Ref. 39. Here U is an SU(2) matrix at link l, V is the "force" at the same link, and $D^J(U)$ ($J=0,\ 1/2,\ 2,\ 3/2,\ \ldots$) is the $(2J+1)$-dimensional, irreducible SU(2) representation. The I_n are modified Bessel functions and we like to remark that Eqs. (9.8.1)–(9.8.3) and (9.6.26) of Ref. 50 allow to write a fast vectorized code. Obviously Eq. (2.33) allows to integrate out expectation values of independent SU(2) link matrices in arbitrary representations. If Polyakov loop correlations at distance $t_z>2$ are considered, all matrices of the two loops are independent. The trial operators for higher units of electric flux (2.32) are, of course, never independent.

As higher representations are obtained with almost no extra effort, we also calculated correlations between Polyakov loops in the $J=\frac{3}{2}$ and $J=2$ representations. For the $\frac{3}{2}$ representation we found as expected the same masses as for $J=\frac{1}{2}$. Similarly, the $J=2$ masses were consistent with those for $J=1$. As in both cases the statistical noise is larger and the projection on the lowest state is smaller for the higher (as compared to the lower) representations, we shall not present these results in detail. When we used the icosahedral subgroup, we replaced $\int dU$ in (2.33) by the explicit sum over all 128 group elements. In that way the calculation of higher representations is very tedious (and $J>1$ representations were not calculated). Additional trial operators were used to calculate masses of glueball states in the T_2^+, T_1^-, and T_2^- representations of the cubic group, but the results remained inconclusive, see Sec. III C.

D. Finite-size scaling and finite-size problems

Quite generally Fisher's scaling variable is defined by Eq. (1.1). However, for analyzing numerical data, it is convenient to associate with each calculated mass m its

own scaling variable $z_m = mL$. The reason is that different masses will be afflicted by rather different statistical and systematical errors. For instance for an analysis of asymptotic scaling, z_m will allow to analyze each mass within its own accuracy. For mass ratios one may use the z_m of the less noisy mass. Our generic notation for z_m will be z.

Let us list the z definitions used in our papers. Following the notation of Ref. 24 we introduce

$$z_0 = m(A_1^{++})L \quad \text{and} \quad z_2 = m(E^{++})L \ . \tag{2.34}$$

In case of the string tension we use

$$z_\kappa = \sqrt{\kappa} L \ , \tag{2.35a}$$

and at one occasion also the alternative variable

$$z_{E_1} = E_1 L = \kappa L^2 \ . \tag{2.35b}$$

Our next two z variables are appropriate for discussing the deconfining phase transition. The conventional discussion uses $L_t L^3$ lattices ($L \to \infty$) and we define

$$z_T^1 = T_c L \quad (L = L_z) \ . \tag{2.36a}$$

As in previous work,[51,52] we consider in this paper T_c signals on $L^2 L_z L_t$ lattices ($L_z \gg L$, $L \to \infty$). We distinguish this from the conventional case by introducing

$$z_T = z_T^2 = T_c L \quad (L \ll L_z) \ . \tag{2.36b}$$

Fisher's scaling limit (1.3) is defined by $z = \text{const}$, $L \to \infty$. In this limit we obtain for each z value the physics of a finite continuous box.

In the limit of large volumes the finite-volume corrections are for glueballs given by Eq. (1.4). In the present investigation we are primarily concerned with mass ratios. Let $R(z) = m_1(z)/m_2(z)$ and $z = z_{m_1}$ or z_{m_2}, Eq. (1.4) yields

$$R(z) = R(\infty) + c_{12} \exp\left[-\frac{\sqrt{3}}{2} z\right] + \text{higher orders in } z, \quad z \to \infty \ , \tag{2.37}$$

where the constant c_{12} can be positive or negative.

Whereas the finite-volume corrections for glueballs are exponentially small, the infinite-volume approach of the string tension is much slower. Possibly large power-law corrections are involved:

$$\kappa(\infty) - \kappa(z_\kappa) = \kappa(\infty)\left[\frac{c_\kappa}{z_k^2} + O\left[\frac{1}{z_\kappa^4}\right]\right] \ . \tag{2.38a}$$

Involving string theory[38,53] the conjecture for the constant is

$$c_\kappa = \frac{\pi}{3} \ . \tag{2.38b}$$

We conclude this subsection with a comment on large lattices versus large volumes. Gutbrod[54] calculated the SU(2) Wilson string tension on a large 24^4 lattice at $\beta = 2.7$ and finds $0.005 < \kappa < 0.011$. In addition, he obtains as strict upper bound $\kappa < 0.0145 \pm 0.001$. In Ref. 4 $\kappa = 0.164 \pm 0.005$ [$\sqrt{\kappa} = (188 \pm 33)\Lambda_L$] was reported for the Polyakov string tension from a $6^3 64$ lattice at $\beta = 2.7$. Comparing this result with his upper bound Gutbrod concluded that a $6^3 64$ lattice is "most likely too small to measure κ reliably." However, the hope is not that a $6^3 64$ lattice approximates infinite-volume physics well, but that it gives a good approximation for the physics of a continuum box with $z_\kappa = L\sqrt{\kappa}$. Figure 2 of Ref. 4 provided some evidence for this, because a $4^3 64$ lattice with $\beta = 2.55$ gives within the statistical accuracy results identical with the $6^3 64$ lattice at $\beta = 2.7$. For our $6^3 64$ lattice we have $z_\kappa(L^3 L_t = 6^3 64, \beta = 2.7) = 0.768 \pm 0.012$. How does it now compare with Ref. 54? The value $\kappa = 0.011$ ($\sqrt{\kappa} = 49\Lambda_L$) is consistent with Ref. 54 and gives z_κ ($L^3 L_t = 24^3 24, \beta = 2.7) \approx 2.5$. Obviously the z_κ values are quite different. It is now amazing to note that within its (bad) accuracy the large lattice result agrees with values from much smaller lattices, namely, with values from a $12^3 24$ lattice at $\beta = 2.50$ and from a $6^3 16$ lattice at $\beta = 2.25$ (in the range $47.5\Lambda_L$ to $55.8\Lambda_L$ for $\sqrt{\kappa}$), see Table III a (below) in Sec. III B. The seemingly very large lattice 24^4 finds itself not close to $z = \infty$, but at a moderate z value in the neighborhood of data points from rather different lattices.

E. Deconfinement phase transition

We shall denote the critical (infinite-volume) deconfinement temperature by T_c^∞. Simulations on finite systems are faced with two problems.

(i) Find *signals* for the finite system that are indicators for the phase transition. We will use the symbol T_c^i for such signals. The index i is to label different signals and will be suppressed, if the signal used is obvious from the context.

(ii) Carry out the extrapolation to the infinite-volume limit $L = \infty$.

Any quantity that gives well-defined numbers on finite systems and approaches T_c^∞ in the infinite-volume limit is a valid definition of a signal (in our sense). It is important not to confuse the signals for the deconfining phase transition with the phase transition itself. There are *no phase transitions on finite lattices.* In agreement with standard use of language in physics, we will freely speak about deconfinement temperature, when we mean a signal for the deconfinement temperature on a finite system. Hence, this deconfinement temperature will depend on lattice size and shape. For instance the standard signal[32] from Polyakov loop expectation values considered on (nonstandard) $L_t L^2 L_z$ lattices moves to $\beta = \infty$ for $L_z \to \infty$ and $L_t L^2$ fixed.[51,52] In contrast, signals constructed from eigenvalues of the (L_z-direction) transfer matrix $\mathcal{T}$ (2.7) are L_z independent and one has to investigate their L dependence. Of particular interest are eigenvalues in nonzero electric charge sectors, because they are directly sensitive to the Z_N central symmetry. If the main aim is to estimate T_c^∞ numerically, one crucial point is of course to optimize the approach to T_c^∞. However, to understand the physics of the system better, it may also be interesting to investigate signals that do not approach T_c^∞ rapidly.

In this paper we focus on tunneling between toron sectors as a signal for the deconfining phase transition. We consider $L_t L^2 \infty$ lattices. Let $\beta_c = \beta_c(L_t)$ correspond to the critical (deconfining) coupling, defined in the limit $L \to \infty$. The finite-size behavior of the energy (2.28) $E_t = E_t(z_T)$ of one unit of 't Hooft electric flux is given by

$$E_t = E_t(\infty)[1 + O(e^{-c_-(\beta) z_T^2})] ,$$

$$c_-(\beta) > 0, \quad z_T \to \infty \quad \text{for } \beta < \beta_c , \tag{2.39a}$$

$$E_t = \frac{c}{z_T} + O\left[\frac{1}{z_T^2}\right], \quad z_T \to \infty \quad \text{for } \beta = \beta_c , \tag{2.39b}$$

and

$$E_t = O(e^{-c_+(\beta) z_T^2}), \quad c_+(\beta) > 0, \quad z_T \to \infty \quad \text{for } \beta > \beta_c . \tag{2.39c}$$

Here z_T is the scaling variable introduced by (2.36b). Ising-model analogies of (2.39a)–(2.39c) are elaborated in Ref. 52. Equations (2.39a) and (2.39c) hold quite generally. They describe usual finite-size corrections for systems with periodic boundary conditions away from the critical point. For instance, (2.39c) can be derived within a simple domains picture for tunneling.[55,52] In contrast, Eq. (2.39b) requires a second-order phase transition. It is instructive to recall the finite-size scaling derivation of (2.39b). We closely follow Ref. 3. Let us keep L_t constant, thus converting the z_T dependence to L dependence, and define

$$t = \frac{g^2 - g_c^2}{g_c^2} = \frac{\beta_c - \beta}{\beta} ,$$

called "reduced temperature" in statistical mechanics. We consider a critical observable $P = P(L,t)$. Critical means that on the infinite system P exhibits the behavior: $P(\infty,t) \sim t^{-\rho}$ $(t \to 0)$, where ρ is the critical exponent of P. An example of P would be the correlation length $\xi = \xi(L,t)$ with critical exponent ν: $\xi(\infty,t) \sim t^{-\nu}$. Fisher's[1] finite-size scaling assumption is

$$\frac{P(L,t)}{P(\infty,t)} = f\left[\frac{L}{\xi(\infty,t)}\right] \quad (L \text{ large, } t \text{ small}) . \tag{2.40a}$$

The $L \to \infty$ limit of the left-hand side immediately implies $\lim_{x\to\infty} f(x) = 1$. In addition, for finite L we have

$$P(L,0) = \lim_{t\to 0} P(L,t) = \text{finite}$$

and the equation

$$P(L,0) = \text{const} \times \lim_{t\to 0}\left[t^{-\rho} f\left[\frac{L}{t^{-\nu}}\right]\right]$$

implies

$$f\left[\frac{L}{\xi(\infty,t)}\right] \sim \left[\frac{L}{t^{-\nu}}\right]^{\rho/\nu}$$

$$\text{for (any) constant } L \text{ and } t \to 0 . \tag{2.40b}$$

Hence,

$$P(L,0) \sim L^{\rho/\nu} \quad \text{for } L \to \infty \tag{2.40c}$$

holds. We are free to choose for P the correlation length itself and get $\xi(L,0) \sim L$ for $(L \to \infty)$, this means $E_t \sim 1/L$.

Equations (2.39a)–(2.39c) imply that $\beta = \beta_c$ becomes in the limit $z_T \to \infty$ a fixed point of the curves $f_{z_T}(\beta) = z_T E(\beta; z_T)$. This is a suitable way to estimate β_c from MC data for $E(\beta; z_T)$. By linearization around the fixed point one obtains the equation

$$\nu = \frac{\ln\left[\dfrac{L'}{L}\right]}{\ln\left[\dfrac{\dfrac{d}{d\beta}[L' m(L',\beta)]_{\beta=\beta_c}}{\dfrac{d}{d\beta}[L m(L,\beta)]_{\beta=\beta_c}}\right]} \tag{2.41}$$

for the critical exponent ν.

F. The lattice β function

At finite z the lattice size L is of order or even smaller than the correlation length and it becomes possible to obtain numerically precise results for large values of the coupling constant β that are not accessible by an infinite-volume calculation $(L \gg \xi)$. Our string-tension results turn out to be precise enough to enable an investigation of asymptotic scaling and its corrections. Similar concepts were previously explored for the two-dimensional O(3) σ model.[56]

In Monte Carlo renormalization-group investigations $\Delta\beta(\beta)$ is often defined as the change in β that increases the correlation length by a factor of 2:

$$\xi(\beta) = 2\xi(\beta - \Delta\beta) . \tag{2.42}$$

Here the definition of the argument β in $\Delta\beta(\beta)$ follows the convention of Hasenfratz[57] to take for β the upper limit of the interval within which the correlations length doubles. For $\beta \to \infty$ the value of $\Delta\beta(\beta)$ follows from the asymptotic scaling formula (2.4b) to be

$$\Delta\beta(\beta) = 4N\beta_0 \ln 2\left[1 + \frac{2N\beta_1}{\beta_0}\frac{1}{\beta} + O\left[\frac{1}{\beta^2}\right]\right] . \tag{2.43}$$

We define more generally $\Delta\beta^\lambda(\beta)$ as the change in β which increases the correlation length by the factor λ:

$$\xi(\beta) = \lambda\xi(\beta - \Delta\beta^\lambda) . \tag{2.44}$$

The asymptotic $\beta \to \infty$ behavior for $\Delta\beta^\lambda(\beta)$ is obtained by substituting $\ln\lambda$ for $\ln 2$ in (2.43). In accordance with Eq. (2.42) we keep the notation $\Delta\beta$ for $\Delta\beta^2$. Our string-tension data give $\Delta\beta^\lambda$ results with λ typically in the range $1.2 < \lambda \leq 2$. An obvious problem is how to compare $\Delta\beta^\lambda$ results for different values of λ. We do this by transforming $\Delta\beta^\lambda$ into $\Delta\beta$ by means of

$$\Delta\beta = \Delta\beta^\lambda \frac{\ln(2)}{\ln(\lambda)} . \tag{2.45}$$

To understand this equation let us discuss $\Delta\beta^\lambda$ in the case of asymptotic scaling. We define $\Delta\beta^\lambda_{\text{as}}(\beta)$ by means of

$$\Lambda_L(\beta)=\lambda^{-1}\Lambda_L(\beta-\Delta\beta^{\lambda}_{\rm as}) \ . \tag{2.46}$$

For SU(2) the crucial observation is that for $\beta\geq 2.2$ and $1.2<\lambda\leq 2$ the power-law factor in the definition (2.4b) of Λ_L gives only a small correction to Eq. (2.45). In the defined range of β and λ the accuracy of this approximation is never worse than 0.4%. Consequently, when asymptotic scaling is satisfied, the translation by means of (2.45) works fine. However, in case of asymptotic scaling violations, its use is problematical. Imagine for instance that a violation of asymptotic scaling is concentrated in a tiny β interval. With $\lambda=2$ it would become smeared out in the sense that $\Delta\beta(\beta)$ would deviate a little bit from the value of $\Delta\beta_{\rm as}(\beta)$ over a rather large β range, whereas a smaller λ value would give a larger effect concentrated in a smaller β range.

For fixed λ the function $\Delta\beta^{\lambda}(\beta)$ is supposed to be *universal*. This means that as soon as (exponentially small) nonperturbative corrections can be neglected (i.e., as soon as scaling holds), $\Delta\beta^{\lambda}(\beta)$ should not depend on (i) the particular mass used to define the correlation length ξ in (2.44), for instance, $\xi=\sqrt{\kappa^{-1}}$, $m^{-1}_{A_1^+}$, $m^{-1}_{E^+}$,..., and (ii) the z value (with $z=z_\kappa$, $z_{A_1^+}$, z_{E^+}, ...) at which the results are obtained.

The definitions (2.42) and (2.44) follow the convention of Ref. 57. Let us remark that consistency of $\Delta\beta^{\lambda}(\beta)$ with $\Delta\beta^{\lambda}_{\rm as}(\beta)$ means that asymptotic scaling is true (in the average) within the range $[\beta_0,\beta]$ where

$$\beta_0=\beta-\Delta\beta^{\lambda}_{\rm as}(\beta) \ . \tag{2.47}$$

Therefore β_0 would be the optimistic estimate of the β value from which one we may trust asymptotic scaling predictions.

G. Monte Carlo data and error bars

This section deals mainly with the problems of estimating the statistical errors of masses which are determined by spectroscopic analysis of (more or less) noisy correlation functions.

A frequently used estimator (for standard statistics notation see, for instance, Ref. 58) of the (connected) correlation functions $C_{\mathcal{O}}(t_z)$ (2.14a) is

$$C'_{\rm MC}(t_z)=\frac{1}{N}\frac{1}{L_z}\sum_{i=1}^{N}\sum_{z=0}^{L_z-1}[\mathcal{O}_i(t_z\oplus z)\mathcal{O}_i(z)-\theta_{\mathcal{O}}\overline{\mathcal{O}}^2] \ , \tag{2.48}$$

where $t_z\oplus z=(t_z+z)\ \mathrm{mod}(L_z)$ and

$$\theta_{\mathcal{O}}=\begin{cases}1 & \text{if } \langle\mathcal{O}\rangle\neq 0 \ ;\\ 0 & \text{if } \langle\mathcal{O}\rangle=0 \ .\end{cases}$$

The index i corresponds to the ith measurement and N is the number of independent measurements. A problem comes when $\langle\mathcal{O}\rangle\neq 0$. One subtracts the $\overline{\mathcal{O}}^2$ term, where

$$\overline{\mathcal{O}}=\frac{1}{N}\frac{1}{L_z}\sum_{i=1}^{N}\sum_{z=0}^{L_z-1}\mathcal{O}_i(z) \tag{2.49}$$

is the estimator of the expectation value $\langle\mathcal{O}\rangle$. It is well known that $\overline{\mathcal{O}}^2$ is a biased estimator of $\langle\mathcal{O}\rangle^2$. For finite statistics its value is systematically too large

$$\langle\overline{\mathcal{O}}^2\rangle=\langle\mathcal{O}\rangle^2+\frac{1}{N}\langle(\mathcal{O}-\langle\mathcal{O}\rangle)^2\rangle \ .$$

Of course, $\overline{\mathcal{O}}^2$ is a consistent estimator, i.e., $\lim_{N\to\infty}\overline{\mathcal{O}}^2=\langle\mathcal{O}\rangle^2$. Consequently, for connected correlation functions ($\langle\mathcal{O}\rangle\neq 0$) (2.48) is also a biased estimator. In contrast, the estimator

$$C_{\rm MC}(t_z)=\frac{1}{N-1}\frac{1}{L_z}\sum_{i=1}^{N}\sum_{z=0}^{L_z-1}[\mathcal{O}_i(t_z\oplus z)\mathcal{O}_i(z)-\overline{\mathcal{O}}(t_z\oplus z)\overline{\mathcal{O}}(z)] \tag{2.50}$$

is unbiased. The proof is a straightforward adaption of the well-known argument[58] which shows that $s^2=\sum(\mathcal{O}_i-\overline{\mathcal{O}})^2/(N-1)$ is an unbiased estimator of the variance $\sigma^2(\mathcal{O})$. Unfortunately, we found out about $C_{\rm MC}$ too late after data taking.

For MC data subsequent events are correlated. Overlooking these correlations would lead to underestimating the statistical errors. Two standard methods to cope with the problem are by computing the autocorrelation matrix or by binning. Only the latter method is used in our investigation. n (usually but not necessarily) subsequent data define a *bin*. It is convenient to choose the total number of data to be a multiple of n. This means $N=Kn$, where K is the number of bins. For binned data Eq. (2.49) becomes

$$\overline{\mathcal{O}}=\frac{1}{K}\sum_{k=1}^{K}\overline{\mathcal{O}}_k$$

$$\text{where } \overline{\mathcal{O}}_k=\frac{1}{n}\frac{1}{L_z}\sum_{i=1+(k-1)n}^{kn}\sum_{z=0}^{L_z-1}\mathcal{O}_i(z) \tag{2.51}$$

is called *bin average* (of the kth bin). Similarly Eqs. (2.48) and (2.50) are readily generalized.

With K bins the estimator of the variance becomes

$$s^2(\mathcal{O})=\frac{1}{K-1}\sum_{k=1}^{K}(\overline{\mathcal{O}}-\overline{\mathcal{O}}_k)^2 \tag{2.52a}$$

and the corresponding error bar is

$$\bar{s}=\sqrt{s^2(\overline{\mathcal{O}})}=\sqrt{s^2(\mathcal{O})/K} \ . \tag{2.52b}$$

Obviously, the $\overline{\mathcal{O}}_\kappa$ in Eq. (2.52) may be any appropriate bin average, such as, for instance, the $C^k_{\rm MC}(t_z)$ of (2.50). In case (for instance by varying the bin size) that different, normalized weight factors w_k ($\sum_k\omega_k=1$) are involved, the generalization of $s^2(\overline{\mathcal{O}})$ is[59]

$$\bar{s}^2=s^2(\overline{\mathcal{O}})=\frac{1}{K-1}\sum_{k=1}^{K}w_k(\overline{\mathcal{O}}-\overline{\mathcal{O}}_k)^2$$

$$\text{with } \overline{\mathcal{O}}=\sum_{k=1}^{K}w_k\overline{\mathcal{O}}_\kappa \ . \tag{2.52c}$$

In cases where the variance of each $\overline{\mathcal{O}}_k$ is known (for instance, because they are results from different investigations), the combined variance is

$$s^2(\overline{\mathcal{O}})=\sum_{k=1}^{K} w_k^2 s^2(\overline{\mathcal{O}}_k)\ , \tag{2.52d}$$

with $\overline{\mathcal{O}}$ as in (2.52c).

In the following we consider bins of equal weight. To minimize the correlations between the MC data one should use as few bins as possible. The price paid is that with very few bins the statistical significance of the error bar is no longer close to that of the Gaussian normal distribution. Our compromise is to calculate (almost) all our error bars with respect to 20 bins. For 20 normally distributed data the student[58,59] distribution gives then the following statistical probabilities for the (unknown) exact results to be within the quoted multiples of the error bars:

$$\begin{aligned} &0.670\ (1\bar{s}),\quad 0.940\ (2\bar{s})\ ,\\ &0.9926\ (3\bar{s}),\quad \text{and } 0.999\,23\ (4\bar{s})\ . \end{aligned} \tag{2.53}$$

This is very close to the Gaussian values for a normal distribution

$$\begin{aligned} &0.683\ (1\sigma),\quad 0.955(2\sigma)\ ,\\ &0.9973\ (3\sigma),\quad \text{and } 0.999\,94\ (4\sigma)\ , \end{aligned}$$

but the probability of a spurious (very unlikely) result is considerably enhanced. For instance, the likelihood to find an event outside the $4\bar{s}$ range is more than 10 times larger with 20 events than it is for a normal distribution.

For correlation functions our reduction of each data set to 20 bins generally provides us with a sample of 20 (almost) normally distributed data. However, the spectroscopic analysis of correlation functions has in addition *bias* problems. To calculate effective masses by means of Eq. (2.14b) we need estimates for ratios of correlations functions

$$R_{\mathrm{MC}}(t_z)=\frac{C_{\mathrm{MC}}(t_z)}{C_{\mathrm{MC}}(t_z-1)}\ . \tag{2.54}$$

Already at this level the bias problem shows up and let us remark that it tends to become much more severe when (sophisticated) fit procedures are used. We now elaborate the problem for $R_{\mathrm{MC}}(t_z)$. As the subsequent correlations functions $C_{\mathrm{MC}}(t_z-1)$ and $C_{\mathrm{MC}}(t_z)$ are strongly correlated, standard error propagation formulas are not at all suitable to calculate the error bar of $R_{\mathrm{MC}}(t_z)$. Instead, one better estimates the error of $R_{\mathrm{MC}}(t_z)$ by binning the ratios itself, as done for the correlation functions by means of Eq. (2.51). However, at large t_z the signal for the correlations sooner or later disappears within the statistical noise and the consequences are disastrous as soon as fluctuations allow $R^k_{\mathrm{MC}}\approx 0/0$. Obviously, this problem becomes first severe for single bins and only at even larger t_z values for the entire statistics. In the latter case the data are useless. But, typical for our investigation is that the problem may exist for single bins, whereas the complete statistics is almost without such bias. In such a situation the "jackknife" method (for a review see Ref. 60) is well suited to estimate the statistical error reliably.

The jackknife method replaces Eq. (2.52a) by

$$s_J^2(\mathcal{O})=(K-1)\sum_{k=1}^{K}(\overline{\mathcal{O}}-\hat{\mathcal{O}}_k)^2\ , \tag{2.55a}$$

where the subscript J stands for "jackknife" and

$$\hat{\mathcal{O}}_k=\frac{1}{K-1}\sum_{i\neq k}\overline{\mathcal{O}}_i\ . \tag{2.55b}$$

It is easily checked that for an unbiased estimator such as (2.49) $s_J^2=s^2$, whereas for a biased estimator s_J^2 is superior to s^2. The jackknife method uses then $R_{\mathrm{MC}}(t_z)$ and

$$\hat{R}^k_{\mathrm{MC}}(t_z)=\frac{\hat{C}^k_{\mathrm{MC}}(t_z)}{\hat{C}^k_{\mathrm{MC}}(t_z-1)}\ , \tag{2.56}$$

where the $\hat{C}^k_{\mathrm{MC}}$ quantities are defined in an obvious way. As $R_{\mathrm{MC}}(t_z)$ is a consistent estimator, the bias of $\hat{R}^k_{\mathrm{MC}}(t_z)$ is (much) smaller than it is for

$$R^k_{\mathrm{MC}}(t_z)=\frac{C^k_{\mathrm{MC}}(t_z)}{C^k_{\mathrm{MC}}(t_z-1)}\ . \tag{2.57}$$

Hence, Eqs. (2.55) give a more reliable error estimate than Eqs. (2.52) do. In our applications the bias of the $\hat{R}^k_{\mathrm{MC}}$ is typically small enough to be neglected altogether. An estimate of the bias can be obtained by comparing the biased mean value

$$R^{\mathrm{biased}}_{\mathrm{MC}}(t_z)=\frac{1}{K}\sum_{k=1}^{K} R^k_{\mathrm{MC}}(t_z) \tag{2.58}$$

with the least biased definition (2.54). Similarly, one proceeds and applies the jackknife method directly to effective masses, mass ratios, etc. An even more detailed analysis would construct the bootstrap[60] probability distribution for each data set. Within our applications this seems not to be worthwhile. Previously jackknife and bootstrap methods have been successfully applied to hadronic spectrum calculations in lattice gauge theories.[61]

III. NUMERICAL RESULTS

In this section we present our complete SU(2) results. Table I gives an overview of the statistics that we rely on. Measurements are done typically every ten sweeps and the first 2000 sweeps are omitted to equilibrate the system, but the actual number may vary for a few data sets. The measurements were DLR improved.[45] At intermediate and smaller β values this was crucial to gain a satisfactory precision. For the sake of completeness we also include data from Refs. 47, 4, 5, and 11, where the icosahedral subgroup[62] was used. Our new data were in part produced with the icosahedral subgroup and in part with the full SU(2) group. Two data sets with the full group use a cold wall[45,47] source. Otherwise we did not use sources. The string-tension data of Sec. III A show that the efficiency (signal over noise ratio) was not improved by use of the source. Supplementary data, discussed in Secs. III C and III E, were taken after we finished the main investigation in order to clarify some physical questions of recent interest. With the exception of Ref. 11, where a mixed fundamental-adjoint action[63]

TABLE I. Overview of data. We give an overview of the data which are analyzed in this paper. They are ordered by (a) lattice sizes and (b) β values. An exception are the data from $L_t L^2 \infty$ lattices, ordered by (a) β values and (b) lattice sizes (as we want to infer on β_c from the L dependence). The statistics is given in kilo (=1000) sweeps. Normally a cold start and 2000 (=$2k$) sweeps to reach equilibrium are done. If the β value is marked by (H) a hot start and 2000 sweeps to reach equilibrium are done. (The number of equilibrium sweeps is larger in case of the mixed action data.[11]) Nearly all our simulations used the congruential random number generator. A few exceptions, marked by (S), used the shift-register random-number generator (see Appendix B for details).

	Lattice	β	Sweeps		Lattice	β	Sweeps
			Isosahedral SU(2) subgroup (Ref. 47)				
01	$6^3 24$	2.30	$35K$	03	$8^3 24$	2.30	$26k$
02	$6^3 24$	2.50	$35K$	04	$8^3 24$	2.50	$35k$
				05	$12^3 24$	2.50	$15k$
			Icosahedral SU(2) subgroup (Ref. 4)				
01	$2^3 16$	2.25	$120k$	08	$4^3 64$	2.70	$120k$
02	$2^3 32$	2.40	$120k$	09	$4^3 64$	2.85	$065k$
03	$2^3 32$	2.55	$130k$	10	$6^3 16$	2.25	$060k$
04	$2^3 60$	2.75	$120k$	11	$6^3 24$	2.40	$120k$
05	$4^3 16$	2.25	$130k$	12	$6^3 32$	2.55	$120k$
06	$4^3 24$	2.40	$210k$	13	$6^3 64$	2.70	$145k$
07	$4^3 32$	2.55	$120k$	14	$6^3 64$	2.85	$055k$
			Icosahedral SU(2) subgroup (new data)				
01	$4^2 24$	2.25	$1252k$[a]	07	$8^3 32$	2.55	$322k$
02	$4^3 24$	2.40	$1202k$[a]	08	$8^3 32$	2.70	$324k$[a]
03	$4^3 64$	2.70	$402k$[a]	09	$8^3 32$	3.00	$324k$[a]
04	$6^3 32$	2.40	$402k$[a]	10	$10^3 32$	2.40	$162k$
05	$8^3 32$	2.40	$402k$	11	$12^3 32$	2.55	$244k$
06	$8^3 32$	2.45	$162k$				
			Icosahedral SU(2) subgroup, mixed action (Ref. 11)				
			$\beta=\beta_F$, $\beta_A=-0.32\beta_F$				
01	$4^3 64$	3.20	$400k$	03	$4^3 64$	3.40	$240k$
02	$4^3 64$	3.20	$240k$				
			$\beta=\beta_F$, $\beta_A=-0.36\beta_F$				
04	$4^3 64$	2.80	$280k$	09	$4^3 128$	4.40	$240k$
05	$4^3 64$	3.20	$280k$	10	$6^3 48$	3.20	$280k$
06	$4^3 96$	3.60	$200k$	11	$8^3 48$	3.20	$160k$
07	$4^3 96$	3.80	$200k$	12	$8^3 48$	3.60	$200k$
08	$4^3 128$	4.00	$240k$	13	$8^3 48$	4.00	$200k$
				14	$8^3 48$	4.40	$200k$
			Full SU(2) group (new data)				
01	$4^3 64$	2.30	$060k$	19	$4^3 128$	3.00	$160k$
02	$4^3 24$	2.40	$644k$	20	$4^3 128$	3.50	$240k$
03	$4^3 24$	2.40	$240k$[b]	21	$4^3 128$	4.00	$240k$
04	$4^3 32$	2.70	$488k$	22	$4^3 128$	4.50	$248k$
05	$4^3 64$	2.70	$640k$	23	$4^3 128$	4.50	$240k$
06	$4^3 16$	3.00	$640k$	24	$4^3 256$	4.50(H)	$320k$
07	$4^3 16$	3.00(H)	$640k$	25	$4^3 256$	4.50	$296k$
08	$4^3 16$	3.00	$640k$	26	$6^3 64$	2.40	$120k$
09	$4^3 24$	3.00	$202k$	27	$6^3 64$	2.40(H)	$100k$
10	$4^3 32$	3.00	$320k$	28	$6^3 64$	2.40(S)	$100k$
11	$4^3 32$	3.00	$320k$	29	$6^3 64$	2.50	$200k$
12	$4^3 64$	3.00	$158k$	30	$6^3 64$	2.70(S,H)	$078k$
13	$4^3 64$	3.00	$320k$	31	$6^3 64$	3.00(H)	$108k$
14	$4^3 64$	3.00(H)	$240k$	32	$6^3 64$	3.00(S,H)	$100k$
15	$4^3 64$	3.00	$320k$	33	$8^3 64$	2.50	$100k$
16	$4^3 64$	3.00(S)	$256k$	34	$8^3 64$	2.70	$100k$
17	$4^3 128$	3.00	$320k$	35	$8^3 64$	3.00(S,H)	$100k$
18	$4^3 128$	3.00(H)	$160k$	36	$10^3 64$	3.00(S,H)	$112k$

TABLE I. (*Continued.*)

	Lattice	β	Sweeps		Lattice	β	Sweeps
			Full SU(2) group (cold wall)				
01	$6^3 64$	2.40	160k	02	$10^3 64$	2.40	080k
			Full SU(2) group ($L_t L^2 \infty$ lattices)				
01	$4\ 4^2 64$	2.28	60k	19	$4\ 6^2 64$	2.34	060k
02	$4\ 6^2 64$	2.28	60k	20	$4\ 8^2 64$	2.34	099k
03	$4\ 8^2 64$	2.28	60k	21	$4\ 10^2 64$	2.34	056k
04	$4\ 10^2 64$	2.28	45k	22	$4\ 12^2 64$	2.34	060k
05	$4\ 12^2 64$	2.28	18k	23	$4\ 16^2 64$	2.34	038k
06	$4\ 4^2 64$	2.30	60k	24	$4\ 4^2 64$	2.36	060k
07	$4\ 6^2 64$	2.30	60k	25	$4\ 6^2 64$	2.36	060k
08	$4\ 8^2 64$	2.30	63k	26	$4\ 8^2 64$	2.36	072k
09	$4\ 10^2 64$	2.30	67k	27	$4\ 4^2 64$	2.38	060k
10	$4\ 12^2 64$	2.30	60k	28	$4\ 6^2 64$	2.38	060k
11	$4\ 16^2 64$	2.30	58k	29	$4\ 8^2 64$	2.38	063k
12	$4\ 4^2 64$	2.32	72k	30	$4\ 4^2 64$	2.41	108k
13	$4\ 6^2 64$	2.32	60k	31	$4\ 6^2 64$	2.41	060k
14	$4\ 8^2 64$	2.32	90k	32	$4\ 4^2 64$	2.45	096k
15	$4\ 10^2 64$	2.32	45k	33	$4\ 6^2 64$	2.45	060k
16	$4\ 12^2 64$	2.32	30k	34	$4\ 4^2 64$	2.50	060k
17	$4\ 16^2 64$	2.32	23k	35	$4\ 6^2 64$	2.50	060k
18	$4\ 4^2 64$	2.34	60k	36	$4\ 4^2 64$	2.70	064k
				37	$4\ 6^2 64$	2.70	060k
			Full SU(2) group (supplementary data)				
01	$4^3 64$	2.15	180k	07	$4^3 64$	2.40	090k
02	$4^3 64$	2.15	100k	08	$4^3 64$	2.50	095k
03	$4^3 64$	2.15	100k	09	$4^3 64$	2.70	095k
04	$4^3 64$	2.20	145k	10	$4^3 64$	3.00	100k
05	$4^3 64$	2.25	100k	11	$6^3 64$	2.50	120k
06	$4^3 64$	2.30	095k	12	$6^3 64$	2.70	110k

[a]Runs from Ref. 5 with extended statistics.
[b]Relies on 64-bit arithmetic.

was used, all results reported in this paper rely on the standard Wilson action (2.1b).

For the full SU(2) group our computer code is, in essence, a simplified version of the SU(3) program published later in Ref. 64. The calculations were done on Florida State University's two pipe Cyber 205. On this computer the SU(2) program runs with an update time of approximately 6.9 μs per link (half-precision) and 9.9 μs per link (full precision). The speed of our 6-hit Metropolis program for the icosahedral group is 5.6 μs per link. We use the CDC UPDATE facility and the computer program is written such that a parameter change in the UPDATE file allows to switch from half-precision to full precision. Production runs were almost exclusively done in half-precision.

A. Raw data

Our "raw" data are measurements of correlation functions. From those we calculate effective masses (2.14b). The large number of effective masses prohibits a complete documentation. Instead, the purpose of this subsection is (i) to illustrate the quality of data for typical cases, (ii) to elaborate on box-temperature problems, and (iii) to comment on various other error sources which we considered.

Table II gives effective masses and ratios for some typical cases. We call effective masses at different distances "consistent" as long as they overlap within their error bars. When we find consistent masses over a "relevant distance" range, we take one of the first masses of this t_z range (and its error bar) as estimate of the asymptotic ($t_z = \infty$) mass. Unfortunately, the relevant distance range is a somewhat subjective concept. It is determined by the largest t_z value for which we still consider the effective mass value to be sensible. If a t_z value exists at which the effective mass increases, as compared with $m(t_z - 1)$, then $t_z - 1$ is a natural choice for the last relevant distance. Namely, such an increase is in contradiction with general principles and hence reflects that the inaccuracy of the data points has become larger than

TABLE II. (a) Icosahedral subgroup, effective masses for $\beta=2.7$, $L^3L_z=4^364$, 402 000 sweeps. (b) SU(2) full group, effective masses for $\beta=2.7$, $L^3L_z=4^364$, 640 000 sweeps. (c) SU(2) full group, effective masses for $\beta=2.50$, $L^3L_z=8^364$, 100 000 sweeps.

t_z	$m(A_1^+)$	$\frac{m(A_1^+)}{m(E^+)}$	t_z	$\sqrt{\kappa}$
		(a)		
01	1.523(04)	1.249(04)	01	0.1955(02)
02	0.740(05)	1.281(08)	02	0.1649(04)
03	0.678(06)	1.255(11)	03	0.1612(06)
04	0.659(11)	1.238(21)	04	0.1602(08)
05	0.646(19)	1.224(36)	05	0.1597(10)
06	0.619(32)	1.173(60)	06	0.1593(12)
07	0.57(06)	1.11(11)	07	0.1588(15)
08	0.57(08)	1.19(20)	08	0.1586(18)
09	0.57(17)	1.23(43)	09	0.1583(21)
10	Noise	Noise	10	0.1580(24)
			11	0.1578(28)
			12	0.1575(31)
			13	0.1574(35)
			14	0.1576(39)
	$m(E^+)$	$\frac{\sqrt{\kappa}}{m(E^+)}$	15	0.1576(44)
			16	0.1577(49)
			17	0.1580(54)
01	1.2195(20)	0.1603(03)	18	0.1579(58)
02	0.5777(21)	0.2854(09)	19	0.1575(61)
03	0.5397(33)	0.2987(13)	20	0.1576(66)
04	0.5320(61)	0.3012(27)	21	0.158(08)
05	0.528(10)	0.303(05)	22	0.158(08)
06	0.527(15)	0.302(07)	23	0.158(09)
07	0.514(24)	0.309(13)	24	0.159(10)
08	0.48(04)	0.333(25)	25	0.159(11)
09	0.47(06)	0.339(40)	26	0.159(12)
10	0.46(09)	0.34(07)	27	0.160(13)
11	0.40(12)	0.40(12)	28	0.160(13)
12	Noise	Noise	29	0.160(14)
			30	0.161(14)
			31	0.161(14)
			32	0.163(14)
		(b)		
	$m(A_1^+)$	$\frac{m(A_1^+)}{m(E^+)}$		
01	1.521(03)	1.247(03)	01	0.1965(02)
02	0.745(04)	1.281(07)	02	0.1649(03)
03	0.686(03)	1.249(06)	03	0.1631(04)
04	0.673(05)	1.227(09)	04	0.1625(05)
05	0.689(11)	1.247(21)	05	0.1626(06)
06	0.739(26)	1.318(52)	06	0.1627(07)
07	0.86(08)	1.55(15)	07	0.1628(08)
08	Noise	Noise	08	0.1630(10)
			09	0.1633(11)
			10	0.1638(13)
			11	0.1642(14)
			12	0.1646(16)
			13	0.1650(19)
			14	0.1654(22)
	$m(E^+)$	$\frac{\sqrt{\kappa}}{m(E^+)}$	15	0.1657(25)
			16	0.1662(29)
			17	0.1664(32)
01	1.2197(13)	0.1611(02)	18	0.1664(36)
02	0.5814(11)	0.2836(06)	19	0.1665(41)
03	0.5492(16)	0.2969(09)		

TABLE II. (*Continued.*)

t_z	$m(E^+)$	$\frac{\sqrt{\kappa}}{m(E^+)}$	t_z	$\sqrt{\kappa}$
04	0.5482(27)	0.2965(14)	20	0.1670(46)
05	0.5528(42)	0.2941(21)	21	0.1677(52)
06	0.560(07)	0.2903(37)	22	0.1685(58)
07	0.556(14)	0.293(08)	23	0.1692(64)
08	0.552(27)	0.295(15)	24	0.1696(70)
09	0.554(49)	0.295(27)	25	0.170(08)
10	0.50(09)	0.326(51)	26	0.171(09)
11	0.38(10)	0.43(10)	27	0.171(09)
12	Noise	Noise	28	0.172(10)
			29	0.174(10)
			30	0.175(11)
			31	0.177(11)
			32	0.177(12)

(c)

	$m(A_1^+)$	$\frac{m(A_1^+)}{m(E^+)}$		
01	6.21(23)	1.06(05)	01	0.2862(05)
02	1.13(23)	0.88(20)	02	0.1681(07)
03	0.784(11)	1.11(02)	03	0.1563(08)
04	0.689(30)	1.05(06)	04	0.1535(11)
05	0.670(49)	1.04(07)	05	0.1526(14)
06	0.846(89)	1.41(23)	06	0.1520(18)
07	0.83(21)	1.28(45)	07	0.1513(24)
08	Noise	Noise	08	0.1512(29)
			09	0.1513(34)
	$m(E^+)$	$\frac{\sqrt{\kappa}}{m(E^+)}$	10	0.514(40)
			11	0.1511(47)
			12	0.1503(58)
01	5.85(14)	0.049(02)	13	0.1491(73)
02	1.29(14)	0.131(14)	14	0.1480(92)
03	0.705(09)	0.222(03)		
04	0.654(15)	0.235(05)		
05	0.646(26)	0.236(10)		
06	0.598(62)	0.254(27)		
07	0.65(13)	0.232(45)		
08	0.54(21)	0.279(99)		
09	Noise	Noise		

the correction effects we would like to see. Without such an increase of the effective mass, a spurious decrease (see the evidence for box-temperature effects below) may as well signal the end of the relevant region, but the issue is of course less clear-cut and may be quite tricky. Last, we do not consider data with error larger than 10%. To give some examples: We extract the asymptotic masses $m(A_1^+)=0.659(11)$, $m(E^+)=0.532(6)$, $\sqrt{\kappa}=0.1602(8)$ from Table II(a), $m(A_1^+)=0.673(5)$, $m(E^+)=0.548(3)$, $\sqrt{\kappa}=0.1625(5)$ from Table II(b), and $m(A_1^+)=0.689(30)$, $m(E^+)=0.654(15)$, $\sqrt{\kappa}=0.1524(14)$ from Table II(c). It is notable that mass ratios are often more stable in t_z than each single mass, as the mutual corrections tend to compensate.

In Fig. 2 we plot (for the lattice $8^3 32$ and $\beta=2.70$) the effective masses for each of 20 ordinary (2.57) bins. This illustrates another aspect of the problem to extract asymptotic masses. Within each bin the masses at t_z, t_z+1, t_z+2, ... are strongly correlated. This means that the χ^2 of a least-squares fit to the correlation function does not have its statistical interpretation, but is rather a ridiculously small number. There are several standard ways out. One is to perform a fit using the full correlation matrix to compute χ^2. Another is to make a least-squares fit to $\hat{C}^k_{\mathrm{MC}}(t_z)$ for each biased improved (2.56) bin and to compute the error bar with respect to the final results of these fits. We found it safer to take a single effective mass (at an appropriate distance) and its error bar as the final result. This gives a rather conservative estimate of the error, because one may still expect small improvements by incorporating information from the strongly correlated results at other distances.

Figures 3(a)–3(c) give an overview of our effective masses for all five $8^3 32$ lattices that we simulated using the icosahedral subgroup. The quality of the other effective masses, used for the asymptotic estimates of this

paper, is in most cases better. In case of the glueballs [Fig. 3(a) and 3(b)] we had to omit the lower β values, because the results are too noisy. The crosses and squares correspond to adopting the biased (2.58) and the least biased (2.54) estimates directly to effective masses. The biased result is the direct average of mass values as plotted in Fig. 2. When biased and unbiased estimates are undistinguishable, we have clear evidence that the bias is small on the scale of our statistical errors. Only at large distances substantial discrepancies are sometimes visible and, as expected, the biased result is then above the less biased one. Of course, the less biased results have to be taken for the spectroscopic analysis.

Let us turn to our numerical data on the box-temperature problem. Clear evidence for box-temperature effects is presented in Figs. 4(a) and 4(b). Both figures rely on data from 4^3L_z lattices at $\beta=3.0$, taken with the full SU(2) group. We have 15 such data sets, see Table I (mainly taken to investigate problems with the congruential random-number generator, see Appendix B). Figure 4 uses 14 of those data sets (the data with the shift register random-number generator were later taken for consistency and did not find their way into this figure). The lower six lines in both figures correspond to

$$L_z=16,\ 16,\ 16,\ 24,\ 32,\ \text{and}\ 32\ .$$

They show effective masses $m(t)$ continuously decreasing with t_z, whereas the upper seven lines correspond to

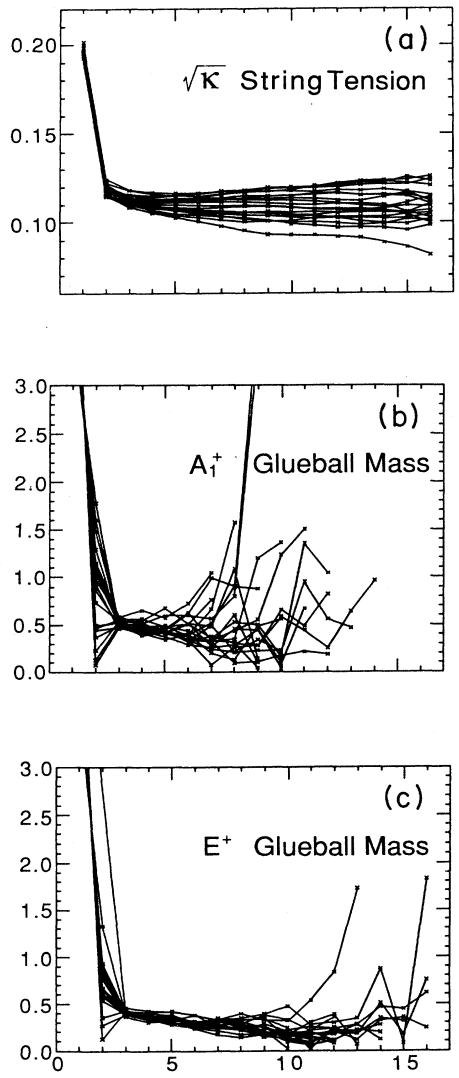

FIG. 2. Effective masses $\sqrt{\kappa}$, $m_{A_1^+}$, and m_{E^+} vs t_z. Each mass is plotted for 20 different bins.

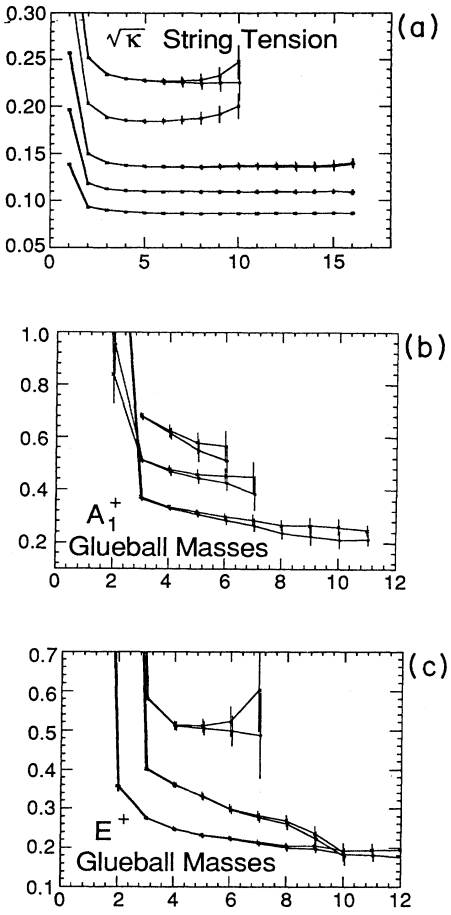

FIG. 3. (a) Effective string tensions, $\sqrt{\kappa}(t_z)$, for our $8^3 32$ lattices (icosahedral group). Biased (2.58) estimates are with crosses, less biased (2.56) estimates are with squares. To guide the eyes the results are connected by straight lines. From up to down, these lines correspond to $\beta=2.40$, 2.45, 2.55, 2.70, and 3.00. (b) Effective A_1^+ glueball masses, $m_{A_1^+}(t_z)$. From up to down, the lines correspond to $\beta=2.55$, 2.70, and 3.00, otherwise as (a). (c) Effective E^+ glueball masses, $m_{E^+}(t_z)$, otherwise as (b).

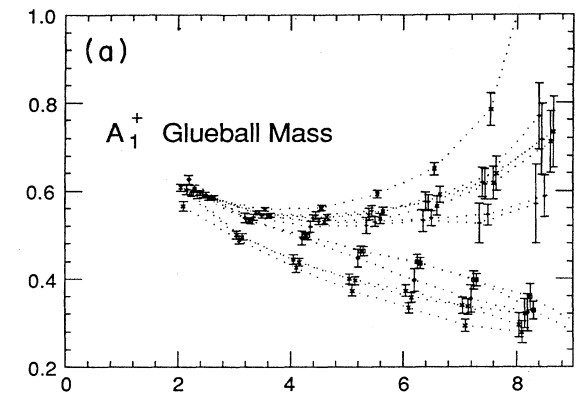

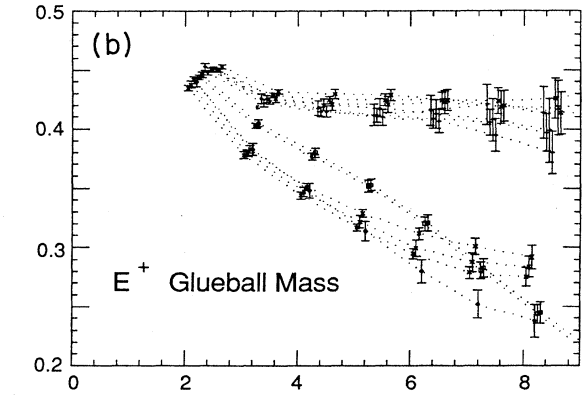

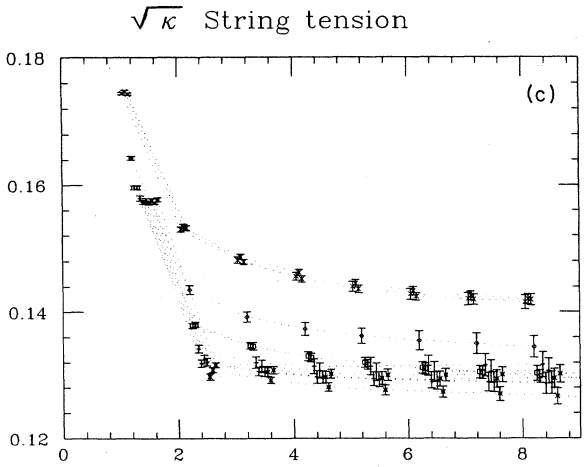

FIG. 4. (a) Effective A_1^+ glueball masses, $m_{A_1^+}(t_z)$, for 4^3L_z lattices and $\beta=3.0$ (full group). The lower branch corresponds to six data sets with $L_z \leq 32$, whereas the upper branch corresponds to six data sets with $L_z \geq 64$. (b) As before, for effective E^+ glueball masses $m_{E^+}(t_z)$. (c) Effective $\sqrt{\kappa}$ string tensions $\sqrt{\kappa}(t_z)$, for 4^3L_z lattices and $\beta=3.0$ (full group). The upper branch corresponds to three data sets with $L_z=16$, whereas the middle branch corresponds to $L_z=24$ and the lower (spread-out) branch corresponds to nine data sets with $L_z \geq 32$.

$L_z=64$, 64, 64, 64, 128, 128, and 128 ,

and show estimates which stabilize for $t_z \geq 4$. Hence, our conclusion is that (with $L=4$ and $\beta=3.0$) $L_z=32$ is not yet large enough to prevent a spurious decrease of effective masses that is obviously due to box temperature. This leads us to reanalyze our mass estimates from the lattices with $L_z \leq 32$. In the present case the effective mass at $t_z=3$ is clearly a much better asymptotic value than the effective mass at, say, distance $t_z=6$. By a technical problem: namely, to avoid paging our lattice in and out of the computer memory, we used nevertheless rather small L_z values for our lattices with $L>4$. Keeping the box-temperature problems in mind, we tried carefully to avoid too large t_z values for our asymptotic estimates. Of course, where to stop is sometimes a rather tedious and subjective decision and very large L_z values would have been more satisfactory.

We also observe box-temperature effects for the string tension. As we are then in the electric charge one sector, the constant a_0 (2.18a) is zero and box-temperature contributions come only from the mass differences with coefficients b_i^n (2.18c). In Fig. 4(c) the effective string-tension estimates for $L_z=16$ are seen to be too high (up to the maximum distance $t_z=8$), whereas for $L_z \geq 32$ values rapid convergence to lower $\sqrt{\kappa}(t_z)$ values is found. The observed effect is therefore opposite to the one found for effective glueball masses. The explanation has to be that a large number of mass differences, each (somewhat) higher than the electric flux energy, contributes to the correlation function. Of course, whether contributing mass differences are smaller or larger than the electric flux energy may depend on lattice size and β value. For instance, at $\beta=2.40$ (6^3L_z lattices) we have evidence for too small effective string tensions caused by box temperature.

We have discarded two of our high-statistics data sets on rather large lattices: namely, the 8^332 data sets at $\beta=2.70$ and 3.00 with 324 000 sweeps each (note that both appear, with lower statistics, in Ref. 5). The fact is that both data sets give results in contradiction with data sets created subsequently on 8^364 lattices [with the full SU(2) group]. Their string-tension results in Table III (a) are in clear contradiction (99% confidence level in each case). The difference is also dramatic for glueball masses, effective mass estimates $m(t)$ with the 8^332 lattices do not stabilize with t [see Figs. 3(b) and 3(c)], whereas the estimates with the 8^364 lattices stabilize. We believe that this is not an effect of the icosahedral approximation (see later) but rather a box-temperature effect as in Figs. 4(a) and 4(b). [We did not feel motivated enough to repeat a run on a 8^332 lattice with the SU(2) group, just to check this point.]

To conclude this section, let us briefly discuss possible sources of systematic errors, namely, choice of a pseudorandom-number generator (see Appendix B), correlations between successive MC configurations, the icosahedral approximation (if used) and rounding errors.

In most cases our statistics are sufficiently large, such that by dividing our complete statistics into 20 bins (see Sec. II G) one washes out correlations between the MC

TABLE III. (a) String-tension results. Asymptotic string-tension estimates for the data summarized in Table I are collected. The numeration of data is identical with Table I. (By various reasons, some of the data of Table I do not show up here; they will be used in other parts of the paper.) In the case of the mixed-action data (Ref. 11) an effective β value is given. Behind β, the number in square brackets gives the "asymptotic" distance t_z at which the string tension is extracted. Plus sign, zero, or minus sign behind t_z indicate whether $\sqrt{\kappa}$ is argued to be a good, neutral, or not so good asymptotic estimate (this information is only available for our new data). (b) Combined string-tension results. String-tension estimates from different investigations, as listed in (a), are combined whenever β value and spatial lattice size coincide. New results from this paper are indicated by [*] in the [Ref.] column. The last column gives the combined statistics and in parentheses the number of data sets combined.

(a)

	Lattice	β [t_z]	$\sqrt{\kappa}$
	Icosahedral subgroup, data from Ref. 47		
01	$6^3 24$	2.30 [4]	0.310(4)
02	$6^3 24$	2.50 [4]	0.167(3)
03	$8^3 24$	2.30 [4]	0.346(12)
04	$8^3 24$	2.50 [4]	0.155(3)
05	$12^3 24$	2.50 [4]	0.170(9)
	Icosahedral subgroup, data from Ref. 4		
01	$2^3 16$	2.25 [5]	0.349(5)
02	$2^3 32$	2.40 [7]	0.298(7)
03	$2^3 32$	2.55 [6]	0.260(3)
04	$2^3 60$	2.75 [8]	0.235(6)
05	$4^3 16$	2.25 [5]	0.331(4)
06	$4^3 24$	2.40 [6]	0.228(5)
07	$4^3 32$	2.55 [5]	0.189(3)
08	$4^3 64$	2.70 [5]	0.161(2)
09	$4^3 64$	2.85 [6]	0.146(5)
10	$6^3 16$	2.25 [4]	0.374(13)
11	$6^3 24$	2.40 [5]	0.210(3)
12	$6^3 32$	2.55 [8]	0.148(3)
13	$6^3 64$	2.70 [5]	0.128(2)
14	$6^3 64$	2.85 [3]	0.114(2)
	Icosahedral subgroup, new data		
01	$4^3 24$	2.25 [4,+]	0.3339(10)
02	$4^3 24$	2.40 [4,+]	0.2308(07)
03	$4^3 64$	2.70 [4,0]	0.1602(08)
04	$6^3 32$	2.40 [4,0]	0.2124(09)
05	$8^3 32$	2.40 [4,+]	0.2293(12)
06	$8^3 32$	2.45 [4,+]	0.1847(16)
07	$8^3 32$	2.55 [5,+]	0.1362(11)
08	$8^3 32$	2.70 [5,+]	0.1097(09), Not used
09	$8^3 32$	3.00 [5,+]	0.0871(07), Not used
10	$10^3 32$	2.40 [4,+]	0.2447(29)
11	$12^3 32$	2.55 [5,+]	0.1327(19)
	Icosahedral subgroup, mixed-action data (Ref. 11)		
01	$4^3 64$	2.202 [4]	0.3003(05)
02	$4^3 64$	2.202 [4]	0.3010(10)
03	$4^3 64$	2.289 [4]	0.2480(10)
04	$4^3 64$	2.083 [4]	0.4350(20)
05	$4^3 64$	2.277 [4]	0.2540(10)
06	$4^3 96$	2.465 [4]	0.1950(10)
07	$4^3 96$	2.557 [5]	0.1780(10)
08	$4^3 128$	2.648 [5]	0.1640(10)
09	$4^3 128$	2.829 [5]	0.1410(10)
10	$6^3 48$	2.277 [4]	0.2540(10)
11	$8^3 48$	2.277 [4]	0.2780(30)
12	$8^3 48$	2.465 [5]	0.1430(20)
13	$8^3 48$	2.648 [5]	0.1070(20)
14	$8^3 48$	2.829 [5]	0.0920(10)

TABLE III. (*Continued*).

(a)

	Lattice	β [t_z]	$\sqrt{\kappa}$	
		Full SU(2) group		
01	$4^3 64$	2.30 [4,+]	0.2883(21)	
02	$4^3 24$	2.40 [4,+]	0.2311(08)	
03	$4^3 24$	2.40 [4,+]	0.2281(12)	64 bits
05	$4^3 64$	2.70 [5,+]	0.1626(06)	
16	$4^3 64$	3.00 [5,+]	0.1278(14)	
17	$4^3 128$	3.00 [5,+]	0.1295(10)	
18	$4^3 128$	3.00 [5,+]	0.1276(08)	
19	$4^3 128$	3.00 [5,+]	0.1300(09)	
20	$4^3 128$	3.50 [5,+]	0.0952(11)	
21	$4^3 128$	4.00 [5,+]	0.0749(11)	
23	$4^3 128$	4.50 [6,0]	0.0593(16)	
24	$4^3 256$	4.50 [6,+]	0.0575(12)	
25	$4^3 256$	4.50 [6,+]	0.0621(13)	
26	$6^3 64$	2.40 [4,0]	0.2146(07)	
27	$6^3 64$	2.40 [4,0]	0.2155(11)	
28	$6^3 64$	2.40 [4,0]	0.2158(14)	
29	$6^3 64$	2.50 [5,0]	0.1630(08)	
30	$6^3 64$	2.70 [5,0]	0.1206(20)	
32	$6^3 64$	3.00 [5,−]	0.0998(15)	
33	$6^3 64$	3.00 [5,0]	0.1005(13)	
34	$8^3 64$	2.50 [5,0]	0.1526(14)	
35	$8^3 64$	2.70 [5,−]	0.1050(14)	
36	$8^3 64$	3.00 [5,0]	0.0813(11)	
37	$10^3 64$	3.00 [5,0]	0.0696(11)	
		With cold-wall source		
01	$6^3 64$	2.40 [5,−]	0.203(6)	
02	$10^3 64$	2.40 [4,−]	0.239(8)	

(b)

	Lattice	β [Ref.]	$\sqrt{\kappa}$	Informations
01	$4^3 L_z$	2.25 [4,5,*]	0.3337(10)	1382k(2)
02	$4^3 L_z$	2.40 [4,5,*]	0.2304(06)	2296k(4)
03	$4^3 L_z$	2.70 [4,5,*]	0.1615(07)	1162k(3)
04	$4^3 L_z$	3.00 [*]	0.1288(06)	0896k(4)
05	$4^3 L_z$	4.50 [*]	0.0596(15)	0856k(3)
06	$6^3 L_z$	2.40 [4,5,*]	0.2136(10)	0842k(5)
07	$6^3 L_z$	2.50 [47,*]	0.1633(08)	0235k(2)
08	$6^3 L_z$	3.00 [*]	0.1001(10)	0208k(2)
09	$8^3 L_z$	2.50 [47,*]	0.1530(13)	0135k(2)

data. A notable exception are our data on $4^3\infty$ lattices at the highest β value $\beta=4.5$, which were taken to study the tunneling transition. In this case 300 000 sweeps are not sufficient to create 20 (almost) independent bins. For the $4^3 256$ lattices the two string-tension estimates of Table III (a) are incompatible (confidence level 98.7%.) A more detailed analysis of these data sets shows that it is not really surprising. The mean value of the Polyakov loops tunnels (change of sign) only about every 45 000 seeps and did not yet converge to the correct value zero. In conclusion, these two estimates obviously have too small error bars and, combining them, a more reliable estimate is of the order of 0.0597(20). We think that our other estimates do not seriously suffer from correlations between the MC-generated events. In addition, our evidence is that we discarded sufficiently many sweeps for equilibration. No systematic bias of the first bin is observed.

By historical reasons a sizable part of our production was done with the icosahedral subgroup approximation to the SU(2) group, for which a scalar computer program is described in Ref. 62. A vectorized version of it was already used in Ref. 47 and could easily be optimized with respect to the Cyber 205. It is generally believed[65] that the icosahedral approximation works well for β values below the first-order phase transition point which one finds at $\beta\approx 5.5$ due to the discreteness of the icosahedral

group. A clear-cut check of the icosahedral approximation can only be done on the $4^3 24$ lattice at $\beta=2.40$ and on the $4^3 64$ lattice at $\beta=2.70$ where we have data on exactly the same lattice size with both icosahedral and SU(2) programs. Some very small effect possibly exists at $\beta=2.70$. It is hard to make a definite conclusion as, even with the unusually high statistics we have assembled, our statistical error estimates are somewhat uncertain (see, e.g., our three different data sets from $4^3 128$ lattices at $\beta=3.00$ with the same program). However, the smallness of the effect of the icosahedral approximation observed on 4^3 lattices at both $\beta=2.40$ and 2.70 is a strong indication that the discrepancies on 8^3 lattices are indeed a box-temperature effect.

Production with the full SU(2) group was done with the half-precision version of our program. We ran the $4^3 24$ data set at $\beta=2.40$ twice in half-precision and full precision. Results are fully compatible. The use of half-precision in the measurement part of our computer code turned out to be more subtle. Indeed, on very long lattices, at the largest β value ($\beta=4.5$), rounding errors spoiled our string-tension estimates with systematic errors, not negligible in comparison with statistical errors. For this reason the string-tension estimate from the first $4^3 128$ lattice at $\beta=4.5$ is omitted. The other runs at $\beta=4.5$ were performed with a version of the computer code using full precision arithmetics in the relevant summations. For lower β values the systematical errors on our final estimates are smaller than the statistical errors.

B. String tension and lattice β function

The string-tension estimates are our most accurate results. In lattice units the results are presented in Table III (a). Let us first comment on the two estimates obtained with the cold-wall source method. Even for the large $10^3 64$ lattice the signal over noise ratio is worse than for the corresponding (icosahedral) data set without source. This tendency is even more drastic in case of the smaller $6^3 64$ lattice. In addition the source introduces new systematic errors, as the approach to the asymptotic ($t_z \to \infty$) values is much slower than without source. Consequently we decided to discontinue production runs with the source method.

Some estimates of Table III (a) correspond to identical lattices and β values. Omitting the source data, we combine data sets whenever the L^3 part of the lattice and the β value agree and these estimates are collected in Table III (b). The given error bar is obtained by means of Eqs. (2.52d) from the individual errors. Comparison with the direct error, obtained by applying (2.52c) directly to the different data sets, gives us a consistency check because these data sets are truly independent. With the exception of the $4^3 L_z$ lattices at $\beta=4.5$ no major inconsistencies are found. In the $\beta=4.5$ case the combined error is too small because of correlations within the individual data sets and instead the direct error is given in Table III (b). (Normally the combined error is the better one, because according to the student distribution it is almost Gaussian.) A slight problem was the optimal assignment of the weight factors in using Eqs. (2.52c) and (2.52d). For runs on identical lattices with identical computer codes the obviously best choice is to take the weight factors proportional to the assembled statistics. However, in case of different computer codes (icosahedral or full group program) and different L_z the optimal choice is less clear. The results of Table III (b) were obtained by comparing three different ways. In two approaches we ignored the possible difference in the efficiency of the computer codes. First, we also ignored the differences in the long (L_z) lattice extension, whereas in the second case we chose the weight factors proportional to L_z. Physically the first case assumes that one lattice configuration is so strongly correlated that no new statistical information is gained by extending L_z, whereas the second case assumes that there is essentially no such correlation and that the statistical information will increase proportional to L_z. (In the limit $L_z \gg \xi$ the second scenario will sooner or later hold.) In our third approach we chose the weight factors proportional to the inverse error bars squared. In principle this takes care of everything, variant efficiencies of the computer code as well as L_z extension. However, in particular for small statistics data sets, this assignment can have problems due to error bar fluctuations. For our actual data no major inconsistencies occurred and with the information from all three approaches the results listed in Table III (b) popped out naturally.

To give a visual impression of our string-tension results, we plot in Fig. 5 the data of Table III (a) in units of Λ_L (a few points are outside the range of the figure). Within rather small violations of asymptotic scaling, the data from differently sized lattices (and hence from different β values) support a universal curve. It is remarkable that this is achieved with data from two different actions.

The $\Lambda_{L(\text{adjoint})}$ scale used for the fundamental-adjoint action is obtained using the formula for the pure Wilson action Λ_L scale with an effective β, as given by the equation

$$\beta_{\text{eff}}=\beta+2\beta_{\text{adjoint}}-\frac{5}{2}\frac{\beta_{\text{adjoint}}}{\beta_{\text{eff}}}$$

(values for β_{eff} are collected in Table III) for more details see Ref. 11. Assuming that the asymptotic large z_κ behavior is given by Eqs. (2.38), and holds from $z_\kappa \approx 1.5$ on, we obtain the estimate

$$\sqrt{\kappa_\infty}=(60\pm 5)\Lambda_L \ . \tag{3.1}$$

Curves according to the upper and the lower limits of this estimate are indicated in the figure. The other solid curve included in the figure is the analytical result by Koller and van Baal.[6,7] In spite of the uncertainties implied by the translation of Λ_{MS} to Λ_L by means of Eq. (2.6), the agreement up to $z_\kappa \approx 1$ is remarkably good. Then the turnover to an increasing string tension is missed by the analytical approach. The results of Fig. 5 are consistent with similar numerical investigations on rather large lattices[15] and also with less accurate earlier

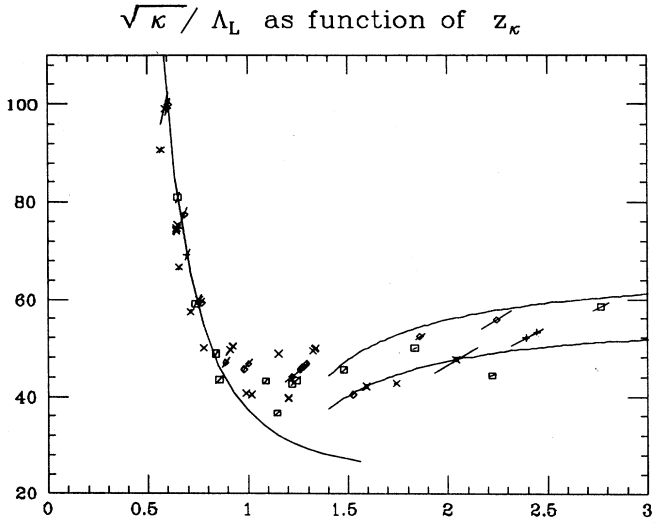

FIG. 5. Plot of string tension results in units of Λ_L (not all data of Table III fit into the figure). The solid line in the small z_κ region is due to Koller and van Baal (Ref. 7). The lines on the right-hand side indicate the upper and lower error bars of the extrapolation (3.1) using the asymptotic equations (2.38). For the data (Ref. 11) with the mixed action we use effective β values given in Table III. Symbols correspond as follows to lattice sizes: vertical cross (2^3L_z), diagional cross (4^3L_z), diamond (6^3L_z), square (8^3L_z), fancy diamond (10^3L_z), and fancy square (12^3L_z). This correspondence between symbols and lattices is also used in subsequent figures.

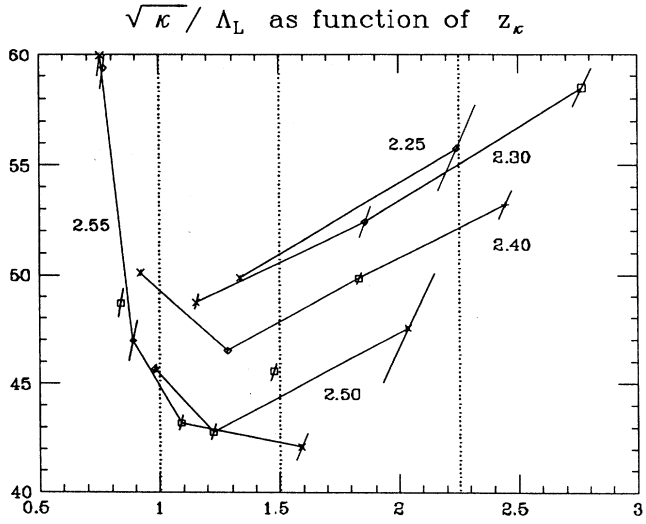

FIG. 6. Enlargement of the central region of Fig. 5. In contrast to Fig. 5 combined data from Table III (b) are used when possible. The straight lines connect results corresponding to identical β values. (The single data point between the $\beta=2.40$ and $\beta=2.50$ line corresponds to $\beta=2.45$.)

result for the 't Hooft string tension, obtained by introducing twist.[66]

The accuracy of our string-tension estimates is good enough to allow a more detailed investigation of asymptotic scaling violations. This part of the analysis is done for the standard action data only. We carry out a determination of the function $\Delta\beta(\beta)$ defined in Sec. II F. The most direct method to read off asymptotic scaling violations is to consider enlargements of Fig. 5. One relevant example is given by Fig. 6, where (in contrast with Fig. 5) the combined data of Table III (b) are used instead of the data of Table III (a) whenever this distinction is meaningful. To guide the eyes results with identical β values are connected by straight lines. At appropriate z_κ values (these are values where we have enough data such that a smooth interpolation can be guaranteed) we read off ratios

$$R(\beta_1,\beta_2)=\frac{\sqrt{\kappa}(\beta_1)/\Lambda_L(\beta_1)}{\sqrt{\kappa}(\beta_2)/\Lambda_L(\beta_2)} . \tag{3.2}$$

These ratios indicate directly deviations from asymptotic scaling. They are summarized in Table IV (a). For the higher β values we used three additional enlargements of Fig. 5 which concentrate on the range $0.5\le z_\kappa\le 0.9$. The error bars are obtained by interpolating upper (or lower) error bar limits of our data points and then treating the lines corresponding to different β values as independent.

The first question to address is: Do our data support a universal lattice β function $\beta_L(g)$ in the range of bare coupling constants we have investigated? The answer is affirmative if we restrict ourselves to lattices of spatial size $L\ge 4$. Finite-lattice-size corrections disappear now within our statistical accuracy, this means we find consistent $R(\beta_1,\beta_2)$ ratios at different z_κ values. (For fixed β larger z_κ values correspond to larger lattices and therefore smaller finite-size corrections, although often larger statistical noise.) Next, we exploit the z_κ independence and calculate $R(\beta_1,\beta_2)$ ratios that are weighted averages over ratios from different (far enough separated) z_κ values. Then, using the definition (2.44) of $\Delta\beta^\lambda(\beta)$ and Eq. (2.45), we calculate estimates of $\Delta\beta(\beta)$ with argument $\beta=\beta_2$. Selected results are given in Fig. 7(a). As in our β range $0.27<\Delta\beta_{as}(\beta)<0.28$, the basic selection principle was to consider differences $\beta_2-\beta_1$ as close as possible to the interval [0.27,0.28]. The data point ($\beta_1=2.25$, $\beta_2=2.30$) is far off from this goal, but as we have no data with $\beta<2.25$ this is our only way to quote a (questionable) result at $\beta=2.30$. With the exception of data point 14 ($\beta_1=2.40$, $\beta_2=2.50$) all our (β_1,β_2) choices are the best possible with the actual data. Data point 14 is included to illustrate the scale factor (λ) dependence of asymptotic scaling violations. It gives the lower of the two estimates at $\beta=2.50$ in Fig. 7(a). This indicates that the deviation from asymptotic scaling is stronger in the range $2.4\le\beta\le 2.5$ than for $2.25\le\beta\le 2.4$.

The "direct" method of analyzing asymptotic scaling violations has two serious disadvantages: (i) The scale factor is not directly controlled (note in particular that for $\beta=2.85$ and 3.00 we have no way to come close to $\lambda=2$); (ii) finite-lattice-size corrections are hidden in the z_κ dependence.

A second method[24] of analysis uses the lattice size L itself to define the scale factor and thus overcomes these difficulties. The starting point is a plot of z_κ vs β as given by Fig. 8. Enlargements of sections of this figure yield directly the $\Delta\beta^\lambda(\beta)$ results of Table IV (b). As before the $\Delta\beta(\beta)$ estimates are then obtained by means of Eq. (2.45). Table IV (b) shows that $L=2$ is too small a spatial lattice size. The remaining estimates with scale factor $\lambda=2$ are condensed into Fig. 7(b), taking the weighted average when two such sets of data exist for one β value. (Data points 2 and 19 are also included in this average, although the scale factor is only $\frac{5}{3}$.) Within their statistical errors Figs. 7(a) and 7(b) exhibit consistent results. Note that Fig. 7(b) still shows deviations from asymptotic scal-

TABLE IV. (a) Asymptotic scaling violations (I). Estimates of ratios $R(\beta_1,\beta_2)$ from string-tension results at various z_κ values. The values from the second $R(\beta_1,\beta_2)$ column are used to calculate $\Delta\beta(\beta)$ for Fig. 7(a); they combine different z_κ values when such data exist. The last column gives the scale factor as defined by Eq. (2.44). (b) Asymptotic scaling violations (II). $\Delta\beta^\lambda(\beta)$ and $\Delta\beta(\beta)$ estimates that follow from enlargements of Fig. 8.

(a)

	β_1	β_2	z_κ	$R(\beta_1,\beta_2)$	$R(\beta_1,\beta_2)$	λ
01	2.25	2.30	1.50	1.010(12)		
02	2.25	2.30	2.25	1.013(36)	1.010(12)	1.15
03	2.25	2.40	1.50	1.069(10)		
04	2.25	2.40	2.25	1.073(37)	1.069(10)	1.56
05	2.25	2.45	1.50	1.114(12)	1.114(12)	1.84
06	2.25	2.50	1.50	1.147(23)	1.147(23)	2.15
07	2.30	2.40	1.50	1.063(10)		
08	2.30	2.40	2.25	1.060(12)		
09	2.30	2.45	1.50	1.107(12)		
10	2.30	2.50	1.50	1.140(23)		
11	2.30	2.55	1.50	1.198(25)	1.198(25)	1.99
12	2.40	2.45	1.50	1.042(09)		
13	2.40	2.50	1.00	1.080(09)		
14	2.40	2.50	1.50	1.072(20)	1.079(09)	1.39
15	2.40	2.55	1.50	1.127(22)		
16	2.45	2.50	1.50	1.029(20)		
17	2.45	2.55	1.50	1.082(22)		
18	2.50	2.55	1.00	1.013(22)		
19	2.50	2.55	1.50	1.051(28)		
20	2.55	2.70	0.80	1.020(64)	1.020(64)	1.49
21	2.70	2.85	0.68	0.903(55)	0.903(55)	1.32
22	2.85	3.00	0.68	1.063(77)		
23	2.85	3.00	0.60	0.963(85)	1.018(57)	1.49

(b)

	L_1 L_2	β	$\Delta\beta^\lambda(\beta)$	$\Delta\beta(\beta)$
01	04 06	2.40	0.131(05)	0.224(09)
02	06 10	2.40	0.176(16)	0.239(22)
03	04 06	2.50	0.126(08)	0.215(14)
04	04 08	2.50	0.220(08)	0.220(08)
05	06 12	2.50	0.223(15)	0.223(15)
06	04 06	2.55	0.119(18)	0.203(31)
07	08 12	2.55	0.116(05)	0.198(09)
08	04 08	2.55	0.221(06)	0.221(06)
09	06 12	2.55	0.205(08)	0.205(08)
10	02 04	2.70	0.305(20)	0.305(20)
11	04 06	2.70	0.161(16)	0.275(28)
12	04 08	2.70	0.226(16)	0.226(16)
13	02 04	2.85	0.356(41)	0.356(41)
14	04 06	2.85	0.204(19)	0.349(33)
15	04 08	2.85	0.288(19)	0.288(19)
16	02 04	3.00	0.356(28)	0.356(28)
17	04 06	3.00	0.193(29)	0.330(50)
18	04 08	3.00	0.306(18)	0.306(18)
19	06 10	3.00	0.172(30)	0.233(41)

ing at $\beta=2.7$. This is not really surprising: With the scale factor $\lambda=2$ the $\Delta\beta(2.7)$ estimate includes data from the region around $\beta\approx 2.5$ where such violations are likely to be present. The $\lambda=1.5$ estimate of $\Delta\beta(2.7)$ in Table IV (b) is already consistent with asymptotic scaling. From $\beta\geq 2.7$ on our data are consistent with asymptotic scaling although the accuracy is somewhat dissatisfying. With appropriately chosen lattices and β values considerable improvements of Table IV (b) would be possible.

The dip observed in Figs. 7 resembles SU(3) results (for a review see Ref. 57). However, compared with SU(3) the effect is small. Our largest deviation from $\Delta\beta_{\rm as}(\beta)$ is about 25%. This result is consistent with previous SU(2) MC renormalization-group calculations[67,68] as well as with an investigation[69] of the potential $V^P_{\rm lat}(t_z)$. The claims of the Wilson string-tension analysis[70] are contradictory, but the analysis of Wilson string-tension data is difficult and it seems that a careful study[69] does not support inconsistencies with our results. In contrast with Refs. 68 and 70, an advantage of our method is that no corrections for "perturbative contributions" are required.

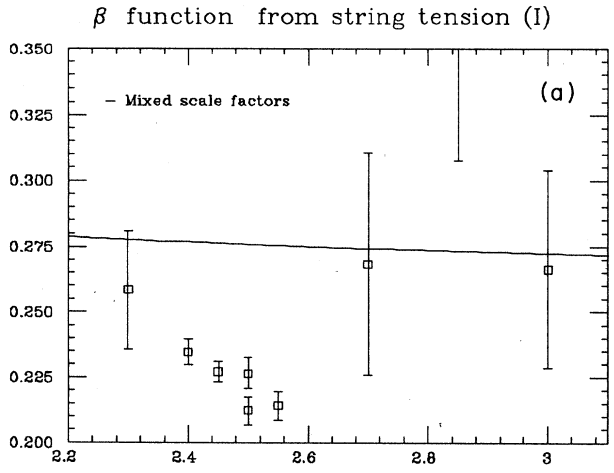

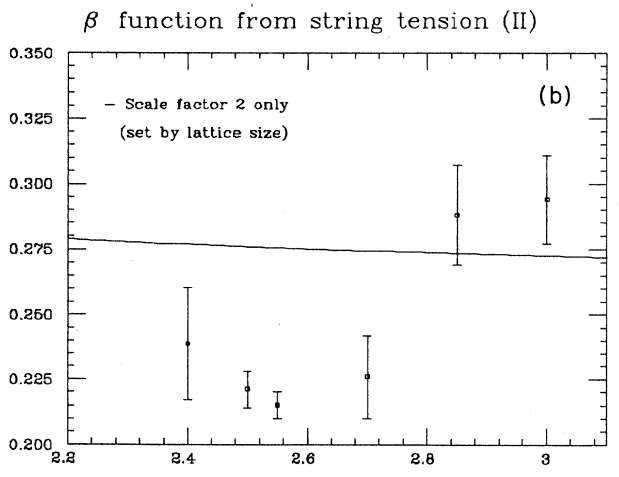

FIG. 7. (a) $\Delta\beta(\beta)$ from string-tension results (first method of analysis as explained in the text). (b) $\Delta\beta(\beta)$ fron string-tension results (second method of analysis as explained in the text).

C. Glueball masses and large volume extrapolations

Table V summarizes the numerical glueball mass estimates as well as the mass ratios $m(A_1^+)/m(E^+)$ and $\sqrt{\kappa}/m(E^+)$. Data of earlier investigations, where either adjoint Polyakov loops were not measured[47] or projections on A_1^+ and E^+ representations were not done,[4] do not show up in this table. In addition, some other data are omitted by various reasons. For instance, some data which allowed a reasonable string-tension estimate, but have a too noisy signal in the glueball sectors. As all masses were measured on the same MC configurations their estimates are correlated. Therefore, the error bars of the mass ratios are not calculated by naive error propagation, but instead by applying the jackknife method (see Sec. II G) directly to these quantities. Sometimes the value chosen for the "asymptotic" distance t_z is slightly smaller than for the string-tension estimate of Table III (a). The reason is that for the less accurate glueball mass data, the large-t_z corrections may disappear earlier within the statistical noise. The accuracy of the glueball estimates is not good enough to allow investigations of asymptotic scaling violations as done in the previous section for the string tension.

For $m(A_1^+)$ our largest reliable values are around $z_0\approx 5$, see Table VI. For the standard action they are well described by

$$m(A_1^+)=(190\pm 10)\,\Lambda_L\ , \tag{3.3}$$

a value consistent with recent literature,[14,15] where results up to much larger volumes, $z_0\approx 15$, are reported. The mixed action prefers a slightly lower value for $m(A_1^+)$. The discrepancy is of the order of expected violations of asymptotic scaling. In the following we con-

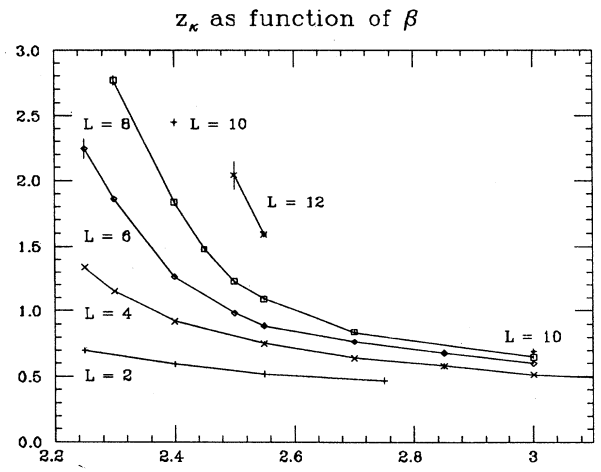

FIG. 8. Plot of z_κ vs β. To guide the eyes identical L values are connected by straight lines. (Exception: $L=10$ because the two data points do not allow a smooth interpolation.)

centrate on analyzing mass ratios in more details. To present our results we choose the scaling variable z_2 because this variable turns out to be less noisy than the otherwise equivalent choice z_0 [a look on Table V shows that our $m(E^+)$ results are systematically better than our $m(A_1^+)$ results]. Altogether our data support universal curves which are consistent with the analytical results. It would be interesting to have results on the violation of scaling (in general), but our data are not precise enough to encourage such an analysis.

Figure 9 plots $\sqrt{\kappa}/m(E^+)$ vs z_2 and provides a detailed comparison with the analytical intermediate-volume result by Koller and van Baal.[6,7] The consistency between the numerical and the analytical approaches is very impressive. However, on the precise scale of Fig. 9, systematic discrepancies are visible as well. Our data

TABLE V. Glueball masses and mass ratios. Asymptotic estimates for glueball masses and mass ratios are given. The numeration of data is identical with Tables I and III (a) (where the lattice sizes and the assembled statistics are also given). Behind β, the number in square brackets gives the "asymptotic" distance t_z at which the mass was extracted.

	β [t_z]	$m(A_1^+)$	$m(E^+)$	$m(A_1^+)/m(E^+)$	$\sqrt{\kappa}/m(E^+)$
		Icosahedral subgroup, new data			
01	2.25 [4]	1.204(64)	1.207(42)	1.00(07)	0.277(10)
02	2.40 [4]	0.936(15)	0.797(12)	1.17(03)	0.290(04)
03	2.70 [4]	0.659(10)	0.532(06)	1.24(03)	0.301(03)
04	2.40 [4]	0.889(37)	0.860(19)	1.03(06)	0.247(05)
07	2.55 [4]	0.613(20)	0.510(11)	1.20(05)	0.269(06)
		Icosahedral subgroup, mixed-action data (Ref. 11)			
01	2.202 [4]	1.25(07)	1.20(04)	1.04(05)	0.251(08)
02	2.202 [4]	1.25(09)	1.17(05)	1.07(09)	0.258(11)
03	2.289 [4]	1.03(03)	0.95(02)	1.09(04)	0.262(05)
04	2.083 [3]	1.76(12)	1.83(11)	0.96(10)	0.238(14)
05	2.277 [3]	1.12(01)	0.95(01)	1.18(02)	0.268(02)
06	2.465 [4]	0.80(01)	0.69(01)	1.16(03)	0.284(03)
07	2.557 [4]	0.73(01)	0.62(01)	1.19(02)	0.289(03)
08	2.648 [4]	0.67(01)	0.55(01)	1.21(02)	0.296(02)
09	2.829 [4]	0.56(01)	0.47(01)	1.20(01)	0.302(02)
10	2.277 [4]	1.12(12)	1.02(05)	1.10(13)	0.250(11)
11	2.277 [3]	1.00(50)	1.60(40)	0.61(40)	0.176(40)
12	2.465 [4]	0.61(02)	0.56(01)	1.08(05)	0.256(06)
13	2.648 [4]	0.46(01)	0.39(01)	1.20(03)	0.279(02)
14	2.829 [4]	0.39(01)	0.29(01)	1.33(03)	0.318(05)
		Full SU(2) group			
01	2.30 [3]	1.183(29)	1.084(19)	1.09(03)	0.266(04)
02	2.40 [4]	0.872(33)	0.760(10)	1.15(05)	0.304(04)
03	2.40 [4]	0.902(39)	0.751(16)	1.20(06)	0.304(06)
05	2.70 [4]	0.673(05)	0.548(03)	1.23(09)	0.297(02)
16	3.00 [4]	0.530(10)	0.412(06)	1.29(04)	0.312(03)
17	3.00 [4]	0.561(06)	0.425(03)	1.32(02)	0.306(02)
18	3.00 [4]	0.530(07)	0.421(05)	1.26(02)	0.304(03)
19	3.00 [4]	0.540(07)	0.430(04)	1.25(02)	0.303(03)
20	3.50 [4]	0.426(05)	0.329(03)	1.29(02)	0.292(03)
21	4.00 [5]	0.360(06)	0.286(03)	1.26(03)	0.259(07)
23	4.50 [5]	0.337(06)	0.270(04)	1.25(03)	0.224(07)
24	4.50 [5]	0.322(04)	0.268(02)	1.20(02)	0.218(05)
25	4.50 [5]	0.317(04)	0.266(02)	1.19(02)	0.235(05)
26	2.40 [4]	0.934(46)	0.835(27)	1.12(08)	0.257(08)
27	2.40 [4]	0.897(47)	0.870(24)	1.03(07)	0.248(06)
29	2.50 [4]	0.697(14)	0.607(08)	1.15(02)	0.270(04)
31	3.00 [4]	0.399(08)	0.316(06)	1.26(03)	0.317(06)
32	3.00 [4]	0.389(08)	0.317(06)	1.23(04)	0.318(04)
33	2.50 [4]	0.689(30)	0.654(15)	1.05(06)	0.235(05)
34	2.70 [4]	0.444(13)	0.387(07)	1.15(04)	0.274(05)
35	3.00 [5]	0.307(09)	0.251(06)	1.22(05)	0.324(09)
36	3.00 [5]	0.280(09)	0.219(06)	1.28(06)	0.318(08)

TABLE VI. $m(A_1^+)$ masses for our largest volumes.

	β	L^3L_z	z_0	$m(A_1^+)/\Lambda_L$
		Mixed-action data (Ref. 6)		
01	2.202	$4^2 64$	5.00(28)	165(10)
04	2.083	$4^3 64$	7.04(48)	173(12)
11	2.277	$8^3 48$	8.00(40)	160(80)
12	2.465	$8^3 48$	4.88(16)	156(06)
		Standard-action data (icosahedral group)		
01	2.25	$4^3 24$	4.82(26)	180(10)
04	2.40	$6^3 32$	5.33(22)	193(09)
07	2.55	$8^3 32$	4.90(17)	194(07)
		Standard-action data (full group)		
01	2.30	$4^3 64$	4.73(12)	200(05)
14	2.40	$6^3 64$	5.60(28)	203(10)
15	2.40	$6^3 64$	5.38(28)	195(10)
16	2.50	$8^3 64$	5.56(09)	195(04)

tend to fall slightly below the analytical curve. Finite lattice spacing corrections to our data and higher-order perturbative (plus other not-well-understood) corrections to the analytical expansion may account for this. Approaching the tunneling transition (coming from large z_2), three of our data points provide evidence for the expected rapid drop of $\sqrt{\kappa}/m(E^+)$. The corresponding z_2 value is somewhat higher than expected from the analytical calculation. Also this discrepancy is not a serious one.

The numerical study of the tunneling transition region is difficult. We had to make a major computational effort in order to reach the transition region on a 4^3L_z lattice. The transition region is located around $\beta=4.5$ and critical slowing down is observed to the extent that 200 000 iterations are not enough on a 4^3256 lattice (see Sec. III A). It would be prohibitively resource consuming to repeat our study of the transition region using larger lattices or to investigate deeper into it with 4^3L_z lattices. Data analysis becomes also quite painful: The fact that the flux energy is rapidly decreasing means that larger and larger L_z's are needed in order to tame finite box-temperature effects. Those are rather dramatic for glueball mass estimates as the signal $\sim\exp(-mt)$ becomes small as compared to box-temperature-induced terms $\sim\exp(-E_1L_z)$ [in the low-z region $m(E^+)\sim m(A_1)\gg E_1$, see Fig. 10]. In addition, it should be noticed that the variational part of the analytical calculation becomes inaccurate when one gets too close to the tunneling transition. In view of these limitations, the agreement found in Fig. 9 is almost marvelous.

Figure 11 presents our $m(A_1^+)/m(E^+)$ ratios. The line on the left-hand side indicates the small volume result.[21] The other solid line is the analytical result for intermediate volumes.[7] Close to the tunneling transition these two lines should match. The figure shows that this is almost achieved, but we notice discrepancies with our MC data in this region. In view of the otherwise very good consistency between analytical and numerical approaches this is somewhat surprising and presently we have no convincing explanation for this disagreement. Possibly the variational part of the analytical calculation, which tends to become bad around the tunneling transition, has more difficulties with an excited state (like A_1^+ is in this approach) than with ground states (like E^+ and κ). Towards larger z_2 values our data are, as before for $\sqrt{\kappa}/m(E^+)$, in very good agreement with the analytical line.

The two dashed curves of Fig. 11 indicate the asymptotic large volume behavior. They are obtained as follows. First, in the range $z_2\geq 2.5$ we make a least-squares fit with our data to the two unknown constants of Eq. (2.37) and obtain $R(\infty)=1.06$, $c_{12}=1.70$. The figure shows that curves with $R(\infty)\pm 0.10$ (and $c_{12}=1.70$) are

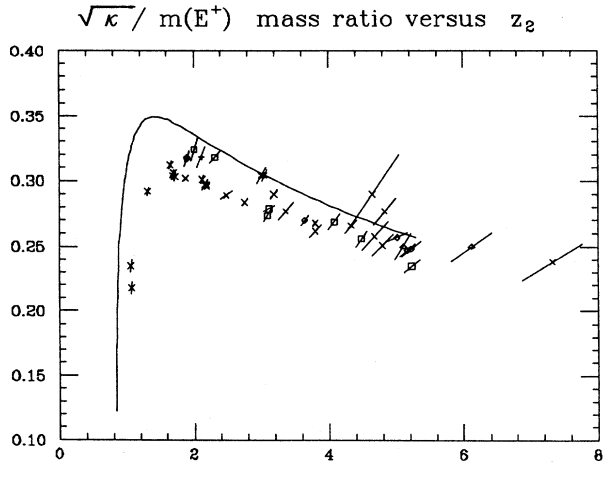

FIG. 9. Plot of $\sqrt{\kappa}/m(E^+)$ vs z_2. The solid line is the analytical result of Koller and van Baal (Ref. 7).

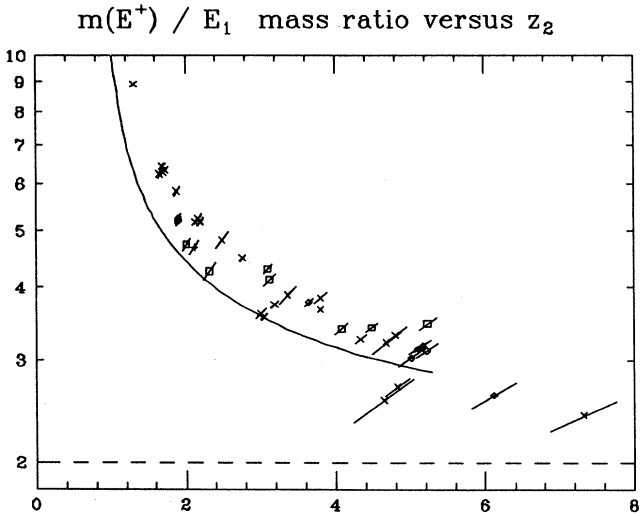

FIG. 10. Semilog plot of $m(E^+)/E_1$ vs z_2. The solid line is the analytical result (Ref. 7).

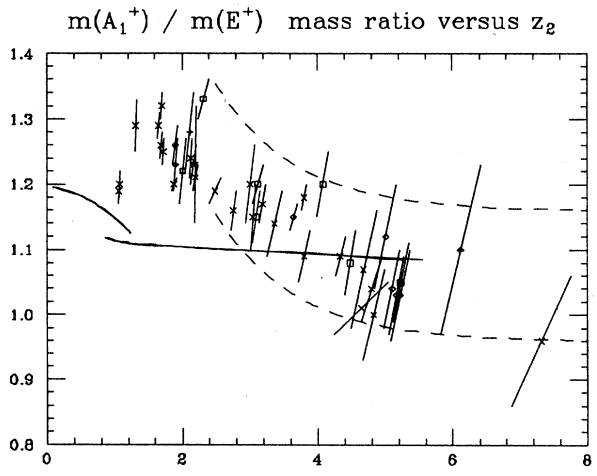

FIG. 11. Plot of $m(A_1^+)/m(E^+)$ vs z_2. The short solid line on the left-hand side is the small volume result of Lüscher and Münster (Ref. 21). The other solid line is the intermediate volume result of Koller and van Baal (Ref. 7). The dashed lines are large volume fits by means of Lüscher's (Ref. 10) equation (2.37).

already envelopes of our data. For the inverse ratio this yields

$$\lim_{z_2\to\infty}\frac{m(E^+)}{m(A_1^+)}=0.95\pm0.10\ . \tag{3.4a}$$

However, although our data are all consistent with these fits and a continuum limit $m(E^+)<m(A_1^+)$ would also be consistent with theoretical constraints,[71] it is nevertheless questionable whether we are allowed to apply the infinite-volume equation (2.37) to $m(A_1^+)/m(E^+)$ in our volume range. The following objections stand against this approach: (i) MC simulations[15] give evidence for $m(E^+)/m(A_1^+)=1.50\pm0.05$ (see Ref. 13 for less convincing earlier results; similar arguments were recently raised in the framework of Hamiltonian variational calculations[82]); (ii) Vohwinkel's[25] analytical calculation and the numerical investigation[72] agree on $m(T_2^+)/m(A_1^+)\approx1.7$ in the intermediate volume range. (T_2^+ is the spin-2 representation alternative to E^+.)

Remark (ii) means that at least one of the spin-2^+ representations of the cubic group is expected to exhibit a significant crossover from intermediate to large volumes. Remark (i) provides evidence that this happens mainly for E^+. Putting both remarks together, the circumstantial evidence is that

$$\lim_{z_2\to\infty}\frac{m(A_1^+)}{m(E^+)}=1.55\pm0.10 \tag{3.4b}$$

holds instead of (3.4a). To confirm this conjecture, further simulations at large volumes are desirable. In view of the large volume results[14,15] for $\sqrt{\kappa}$ and $m(A_1^+)$, we are thus left with a scenario that expects a smooth infinite-volume extrapolation of the $\sqrt{\kappa}/m(A_1^+)$ and, possibly, the $m(T_2^+)/m(A_1^+)$ mass ratio, whereas ratios involving $m(E^+)$ are suspected to exhibit a "crossover" in the range $6<z_2<10$.

Towards larger volumes the asymptotic $\sqrt{\kappa}/m(E^+)$ ratio will be approached from below if Eqs. (2.28) and (1.4) hold. Instead, there is a monotonically decreasing tendency in the z_2 volume range of Fig. 9. By comparison with Fig. 5 it is obvious that this is due to an increasing $m(E^+)$ mass. At our largest z_2 values we have $m(E^+)/m(A_1^+)\approx1$. We may try to extract the asymptotic $\sqrt{\kappa}/m(A_1^+)$ ratio from our results. In view of the rather different large volume corrections for $\sqrt{\kappa}$ (2.38) and $m(A_1^+)$ (1.4), this is best done by taking the ratio of Eqs. (3.1) and (3.3). The result is

$$\lim_{z_0\to\infty}\frac{\sqrt{\kappa}}{m(A_1^+)}=0.315\pm0.030\ . \tag{3.5}$$

Corrections to asymptotic scaling should drop out. Therefore, the reliability of (3.5) is better than for the individual estimates (3.1) and (3.3).

The glueball calculations reported so far were done with the adjoint Polyakov loop. To include more representations of the cubic group we did an exploratory study with two additional Polyakov loop trial operators, denoted $\mathcal{PP}$ and $\mathcal{PAP}$ in the following. Here we use the notation $\mathcal{P}$ for a fundamental- and $\mathcal{A}$ for an adjoint-Polyakov loop. The operator $\mathcal{PP}$ consists of two neighbored, parallel fundamental Polyakov lines and $\mathcal{PAP}$ is made out of three neighbored, parallel Polyakov lines that form a right angle (the Polyakov line in the middle is in the adjoint representation). Figures of these operators are given in Ref. 26. With respect to the cubic group the transformation properties of $\mathcal{PP}$ and $\mathcal{PAP}$ are identical to those of the double plaquette and the bent plaquette. The irreducible representations of these Wilson loops are constructed in Ref. 43 and we can read off from there the irreducible representations of $\mathcal{PP}$ and $\mathcal{PAP}$. For $\mathcal{PP}$ we find A_1^+,E^+,E^+,A_2^+ and $\mathcal{PAP}$ gives $A_1^+,E^+,T_2^+,T_1^-,T_2^-$.

We did MC simulations measuring correlations for all these representations of the cubic group. Unfortunately, the results were somewhat disappointing. The new mass estimates in the A_1^+ and E^+ representation are nicely consistent with previous results, but correlations for all other representations turned out to be inconclusive statistical noise. The latter situation also holds for one of the two E^+ representations of $\mathcal{PP}$. These features are true for all the exploratory data sets (listed in Table I). As this is not very interesting we just illustrate with Table VII the situation for the $4^3 64$ lattice at $\beta=2.70$. In case of the two-dimensional E^+ representation we give results for both components separately, whereas for the three-dimensional T_1 and T_2 representations we pick out the "best" result (upper bounds). A simple heuristic explanation for the noisy signals can be provided. By inspection of the relevant combinations of Polyakov lines, it is found that all noisy operators involve differences of close-by, *parallel* Polyakov loops, such that their expectation values are zero (even in a broken phase). As the Polyakov loops are strongly correlated, these cancellations imply an already small signal at distance $t_z=0$, which just is too tiny to propagate any further.

TABLE VII. Supplementary data. Some effective masses from an attempt to estimate glueballs in variant representations of the cubic group. The results of this table were obtained on a $4^3 64$ lattice at $\beta=2.70$. Behind the error bars, the numbers in square brackets give the distance t_z to which the effective mass corresponds. Note that the operator $\mathcal{PP}$ has two different E^+ representations.

	$\mathcal{A}$	$\mathcal{PP}$		$\mathcal{PAP}$
$m(A_1^+)$:	0.67(17) [4]	0.55(27) [4]		0.61(26) [4]
$m(E^+)$:	0.52(02) [4]	0.52(02) [4]	≤ 3.2 [2]	0.57(05) [4]
	0.58(03) [4]	0.56(02) [4]	≤ 2.5 [2]	0.55 (05) [4]
$m(T_2^+)$:				≤ 11 [1]
$m(A_2^+)$:		≤ 4.1 [1]		
$m(T_1^-)$:				≤ 6.7 [1]
$m(T_2^-)$:				≤ 6.1 [2]

D. Glueballs or flux states?

Arguments[40] were raised that adjoint Polyakov loops are not trial operators for glueballs, but instead for (electric) flux bound states (called "torelons" in Ref. 40). Let us recall from Sec. II G that correlation functions of Polyakov loops in the fundamental representation fall off with the mass $E_1 = L\kappa$ corresponding to one unit of 't Hooft electric flux. The question is now whether some kind of flux bound states may exist in the charge zero sector. For large volumes these hypothetical states would disappear as their mass should rise linearly with L. Decreasing L, one may imagine a level crossing between flux bound states and glueballs. Heuristically, such a picture would be very appealing if the following conditions were true: (i) These bound states exist and have mass

$$E_{[\text{flux bound state}]} \sim 2E_1 \ ; \tag{3.6}$$

(ii) applied to the vacuum, the adjoint Polyakov loop has a large projection onto the flux bound-state wave function.

Our data show that none of these conditions holds. In Fig. 10 we plot $m(E^+)/E_1$ vs z_2. For small z_2 it is seen that this ratio has no tendency to get stable around $m(E^+)/E_1 \sim 2$ but becomes very large. Obviously a similar result holds for $m(A_1^+)/E_1$. The observed mass gaps in the A_1^+ and E^+ representations of the cubic group ignore the decreasing $E_1 = L\kappa$ mass. Hence, there is no support for the existence of flux bound states with mass of order (3.6). The situation is somewhat less clear for increasing $z_2 > 4$. However, we shall demonstrate that in this region the adjoint Polyakov loop couples only weakly to the mass gap state, in contrast with a flux bound-state picture.

How well do our trial operators project the vacuum onto the eigenfunctions of the estimated eigenvalues? Table VIII gives a concise overview and is obtained as follows. Let t_z be the "asymptotic" distance of our best effective mass. The equation

$$p = \prod_{i=0}^{n} \frac{\mathrm{ch}_{m(i)}(1)}{\mathrm{ch}_{m(t_z)}(1)} \quad \text{with } n = t_z - 1 \tag{3.7}$$

estimates the projection of the trial operator. Table VIII gives p (in %) for some characteristic β values and lattice sizes. Let us remark that good upper bounds to the results of Table VIII are often already obtained by using Eq. (3.7) with $t_z = 2$. The p values exhibit the following systematics: (a) For L fixed the projection of the adjoint Polyakov loop increases with increasing β. In case of $L=4$ from $p \approx 8\%$ ($\beta=2.25$) to $p \approx 80\%$ ($\beta=4.50$); (b) the projection of the fundamental Polyakov line is always rather high. For $L=4$ it seems to reach a maximum around $\beta \approx 3.00$ and to decrease then for increasing β; (c) for β fixed and L increasing (see $\beta=2.50$, $L=4,6,8$ and $\beta=3.00$, $L=4,6,8$), the projection of the adjoint Polyakov

TABLE VIII. Projection properties of Polyakov loops. Relying on Eq. (3.7) projection probabilities p of trial operators are estimated. The trial operators are the adjoint Polyakov line for $m(A_1^+)$, $m(E^+)$ and the fundamental Polyakov line for E_1. Behind β, the used distance t_z is given. Results are given in %. The relative errors (omitted) are of the order of a few percent of the result.

L^3	L_z	β [t_z]	$m(A_1^+)$	$m(E^+)$	E_1	Data set
4^3	24	2.25 [4]	7.8%	8.5%	86%	Icos 01
4^3	24	2.40 [4]	18%	22%	91%	Icos 02
4^3	64	2.50 [4]	27%	32%	96%	Full 07 (Suppl.)
6^3	64	2.50 [4]	3.4%	4.2%	86%	Full 30
8^3	64	2.50 [4]	0.2%	0.3%	77%	Full 34 [Table II(c)]
4^3	64	2.70 [4]	39%	49%	95%	Full 05 [Table II(b)]
4^3	64	3.00 [4]	55%	63%	95%	Full 17
6^3	64	3.00 [4]	22%	28%	87%	Full 32
8^3	64	3.00 [5]	5.0%	6.6%	79%	Full 37
4^3	128	4.00 [5]	66%	77%	83%	Full 21
4^3	128	4.50 [5]	71%	79%	72%	Full 23

line decreases strongly, whereas the projection of the fundamental Polyakov line is rather slowly decreasing.

It is amazing to note ($8^3 64$ lattice and $\beta=2.50$) that with a projection of less than 1% the signal of the adjoint Polyakov loop can still be followed far enough to allow a rather clear estimate of the mass gap. In that case the adjoint Polyakov line seems to couple rather "democratically" to all states in the spectrum. Presumably this is related to the fact that it is a nonlocal operator. The gap between the estimated state and the other states is large, which results in a rather rapid convergence of effective masses [see Table II(c)]. For increasing L (β fixed), we find that the adjoint Polyakov loops decouple from the A_1^+ and E^+ mass gap wave functions. We take this as further evidence that these wave functions correspond to glueballs. One is tempted to speculate that for even larger L string formation (see also next section) sets in and the adjoint Polyakov loop may then project dominantly onto a state (above the glueball state) with mass given by (3.6). Concerning investigations with Wilson-loop trial operators, it is instructive to remark that they project differently than adjoint Polyakov loops onto glueball wave functions. Analyzing results from Refs. 12 and 13 it is found that (a) Wilson-loop trial operators have rather high projections ($>30\%$) as long as they work at all and (b) their projection decreases with increasing β (L fixed).

One may also address the question of this section analytically. The intermediate volume results[7] (compare the corresponding curves of Figs. 9 and 10) show a tunneling decrease for E_1, but not for $m(A_1^+)$ or $m(E^+)$. Consequently, the $m(A_1^+)/E_1$ and $m(E^+)/E_1$ mass ratios tend to infinity for $z_2 \to 0$, a result which is highly unfavorable for the hypothesis of flux bound states (at least in the considered limit).

The only evidence for flux bound states comes from strong-coupling expansion ($\beta \to 0$). In lowest order one finds two very distinct ways to correlate adjoint Polyakov loops. Either one covers the spanned area with plaquettes twice and obtains

$$\langle \mathcal{A}(0)\mathcal{A}(t_z)\rangle \sim \beta^{2Lt_z} , \tag{3.8a}$$

corresponding to energy $E_{[\text{flux bound state}]}=2E_1$ (the area has to be covered once to correlate fundamental Polyakov lines[39]), or one covers a connecting tube with plaquettes and obtains

$$\langle \mathcal{A}(0)\mathcal{A}(t_z)\rangle \sim \beta^{4t_z} \quad \text{for } t_z \to \infty . \tag{3.8b}$$

The latter case corresponds to the lowest order of the conventional glueball mass.[73] It should be noted that at this order $E_{[\text{flux bound state}]}(L) > m_{[\text{glueball}]}(L)$ for $L \geq 3$. It would be of some interest to work out higher orders of the strong-coupling expansion for lattices with $L>2$.

E. Deconfinement, tunneling, and string formation

As discussed in Sec. II E we use asymmetric lattices to study the connection between tunneling and deconfinement. We assembled data (see Table I) on $4 \times L^2 64$ lattices. As usual in this paper, Polyakov lines in the fundamental and adjoint representation served as trial operators. We measured momentum zero correlations $\langle \mathcal{P}_i(0)\mathcal{P}_i(t_z)\rangle$ (no summation over i). Because of the asymmetric geometry we have to distinguish between Polyakov lines that close in L_t direction and those that close in L direction. We do this by introducing subscripts t (like "time") and s (like "space") for the corresponding string tensions (2.28) as well as mass gaps. The numerical estimates are collected in Table IX.

The L dependence of κ_t and m_t is analyzed by means of Fig. 12. The left-hand side of this figure plots $LE_t = L_t L \kappa_t$ vs $z_T = L/L_t = L/4$ ($\beta=$const) and is almost a reproduction of Fig. 3 of Ref. 52. (Figure 12 corrects a trivial error of Ref. 52, where all numbers on the abscissa of Fig. 3 have to be multiplied with 16 to agree with the string-tension results given in Table IX.) Relying on Eqs. (2.39a)–(2.39c) we obtain the estimate $2.28 < \beta_c < 2.32$. The right-hand side of Fig. 12 gives the corresponding plot for the mass gap m_t. On both sides of the transition point, the mass m_t has a finite nonzero limit as L grows, and Eq. (2.39a) holds with E_t replaced by m_t. The exponentially small E_t of the broken phase has clearly no analog here, instead we expect a finite screening mass. At the critical point m_t goes to zero although it is not related to the order parameter. The right-hand side of Fig. 12 shows this behavior. For $\beta=2.30$ and 2.32, Lm_t stays approximately constant, whereas Lm_t increases with L for $\beta=2.28$ and 2.34. In this way m_t gives another, perfectly consistent (although less accurate), estimate of the deconfining temperature.

The most accurate calculation of the critical temperature from the 't Hooft electric flux is achieved by exploiting the fixed-point property of Eqs. (2.39a)–(2.39c). Figure 13 depicts LE_t vs β ($L=$const). Obviously, a natural estimate for the fixed points β_c is

$$2.294 \leq \beta_c \leq 2.302 \quad (L_t=4) . \tag{3.9a}$$

This is in good agreement with previous numerical estimates $\beta_c = 2.29 \pm 0.01$ (Ref. 74) and $\beta_c = 2.295 \pm 0.005$ (Ref. 75). These results assume as input Ising-model values for certain critical exponents, whereas our estimate makes no such assumptions. On the contrary, the fixed-point method allows us in principle to go on and to estimate the critical exponent ν, using Eq. (2.41). However, the accuracy of our present electric flux data is not quite sufficient. Approximating the derivatives in Eq. (2.41) from the straight lines in the left part of Fig. 13, we have calculated ν for the various ratios L_2/L_1 with $4 \leq L_1 < L_2 \leq 12$. The obtained values scatter in the range $0.53 \leq \nu \leq 0.71$. This is consistent with the expected 3D Ising-model value $\nu=0.64$ (Ref. 76), but not very conclusive due to lack of accuracy.

Although $L_t=4$ is of course rather small it is quite instructive to translate (3.9a) to units of Λ_L. We get

$$41.6\Lambda_L < T_c < 42.5\Lambda_L \quad (L_t=4) . \tag{3.9b}$$

This is about 20% higher than the analytical estimate,[8] which is $28\Lambda_L < T_c < 35\Lambda_L$. The analytical calculation uses L_t to set the scale. In the lattice regularization

$T_c = 40\Lambda_L$ together with $L_t = 4$ would then correspond to the renormalized coupling $g_{\text{ren}} = 1.52$, whereas $\beta = 2.30$ corresponds to the bare coupling $g_0 = 1.32$. Hence, the bare coupling is somewhat smaller than the renormalized coupling and that is where lattice calculations just begin to make sense (in the continuum limit $g_0 \to 0$ by asymptotic freedom). Not only the numerical but also the analytical T_c estimate suffers presently from a number of more or less uncontrolled error sources. In view of the entirely different systematics of both approaches, the found agreement within about 20% is satisfactory. Although Eq. (2.39b) does not hold for SU(3), we are optimistic that similar methods will work also in that case. The reason is that Eqs. (2.39a) and (2.39c), which still hold, are the really important ones.

For our 4×6^2 64 lattices Fig. 14 demonstrates the tunneling transition. The ratio $\sqrt{\kappa_t}/m_t$ is plotted vs z_{m_t} and should be compared with Fig. 9. As compared to symmetric lattices, the tunneling transition is shifted to a considerably higher z value. In consequence we need only moderately high β values in our simulation. In view of the somewhat large discrepancy with the analytical curve,[8] a finite-size study using $6 \times 12^2 \infty$ lattices may be worthwhile.

Figure 15 plots the spacelike string tension κ_s (2.28) and mass gap m_s the same way as Fig. 12 does for the corresponding timelike quantities. The L dependence is remarkably different. Independently of β, LE_s as well as Lm_s always soar approximately linearly with L. The deconfinement appearing in the behavior of the timelike component of the gauge field does not influence the spatial components in a substantial way, see also Ref. 77. The similarity to permanent confinement in three-dimensional gauge theory[78] is striking.

TABLE IX. Results for the asymmetric lattices. This table gives the estimates from our simulation on $4L^2 64$ lattices. The corresponding statistics can be found in Table I.

	L^2	β	$\sqrt{\kappa_t}$	$\sqrt{\kappa_s}$	m_t	m_s
01	4^2	2.28	0.3067(12) [3]	0.3067(12)[3]	1.229(20) [3]	1.229(20) [3]
02	6^2	2.28	0.2521(23) [3]	0.3480(20)[3]	0.836(15) [3]	1.71(18) [3]
03	8^2	2.28	0.2316(19) [3]	0.3731(37)[3]	0.691(11) [3]	Noise
04	10^2	2.28	0.2229(27) [3]	0.382(08) [3]	0.657(16) [3]	Noise
05	12^2	2.28	0.2131(43) [3]	0.372(35) [3]	0.640(36) [3]	Noise
06	4^2	2.30	0.2882(15) [3]	0.2882(15)[3]	1.110(15) [3]	1.110(15)
07	6^2	2.30	0.2251(24) [3]	0.3255(16)[3]	0.705(25) [4]	1.72(12) [3]
08	8^2	2.30	0.1974(24) [3]	0.3468(20)[3]	0.570(15) [4]	Noise
09	10^2	2.30	0.1713(39) [4]	0.3592(39)[3]	0.467(15) [4]	Noise
10	12^2	2.30	0.1548(34) [4]	0.357(09) [3]	0.369(20) [5]	Noise
11	16^2	2.30	0.1368(47) [4]	0.41(06) [3]	0.307(18) [5]	Noise
12	4^2	2.32	0.2703(18) [4]	0.2703(18)[4]	1.051(13) [3]	1.051(13) [3]
13	6^2	2.32	0.1985(37) [4]	0.3047(16)[3]	0.712(14) [3]	1.550(80) [3]
14	8^2	2.32	0.1534(33) [4]	0.3240(21)[3]	0.512(16) [4]	Noise
15	10^2	2.32	0.1234(47) [4]	0.3385(32)[3]	0.396(13) [4]	Noise
16	12^2	2.32	0.1151(58) [4]	0.358(10) [3]	0.360(20) [4]	Noise
17	16^2	2.32	0.0557(44) [8]	0.321(19) [3]	0.286(25) [6]	Noise
18	4^2	2.34	0.2557(19) [4]	0.2557(19)[4]	0.984(10) [3]	0.984(10) [3]
19	6^2	2.34	0.1797(31) [4]	0.2881(11)[3]	0.649(22) [4]	1.271(45) [3]
20	8^2	2.34	0.1210(44) [5]	0.3076(16)[3]	0.481(10) [4]	Noise
21	10^2	2.34	0.0938(73) [6]	0.3169(25)[3]	0.399(32) [6]	Noise
22	12^2	2.34	0.0495(12) [8]	0.3263(38)[3]	0.462(22) [5]	Noise
23	16^2	2.34	0.0204(42) [15]	0.316(12) [3]	0.404(20) [5]	Noise
24	4^2	2.36	0.2475(18) [4]	0.2475(18)[4]	0.943(10) [3]	0.948(10) [3]
25	6^2	2.36	0.1593(39) [4]	0.2719(16)[3]	0.613(19) [4]	1.258(35) [3]
26	8^2	2.36	0.1091(39) [4]	0.2973(16)[3]	0.514(19) [4]	1.44(19) [3]
27	4^2	2.38	0.2424(23) [4]	0.2424(23)[4]	0.922(08) [3]	0.922(08) [3]
28	6^2	2.38	0.1357(44) [4]	0.2643(16)[4]	0.578(22) [4]	1.227(27) [3]
29	8^2	2.38	0.0732(81) [5]	0.2543(13)[3]	0.589(27) [4]	1.52(13) [3]
30	4^2	2.41	0.2264(14) [4]	0.2264(14)[4]	0.847(08) [3]	0.847(08) [3]
31	6^2	2.41	0.1314(51) [4]	0.2472(13)[3]	0.591(22) [4]	1.090(20) [3]
32	4^2	2.45	0.2119(14) [4]	0.2119(14)[4]	0.788(15) [4]	0.788(15) [4]
33	6^2	2.45	0.1027(56) [4]	0.2368(13)[3]	0.552(20) [4]	1.010(18) [3]
34	4^2	2.50	0.2006(14) [3]	0.2006(14)[3]	0.749(08) [3]	0.749(08) [3]
35	6^2	2.50	0.0756(49) [4]	0.2179(20)[4]	0.568(15) [4]	0.930(16) [3]
36	4^2	2.70	0.1625(09) [4]	0.1625(09)[4]	0.571(04) [4]	0.572(04) [4]
37	6^2	2.70	0.0606(50) [4]	0.1839(23)[4]	0.568(40) [4]	0.728(10) [3]

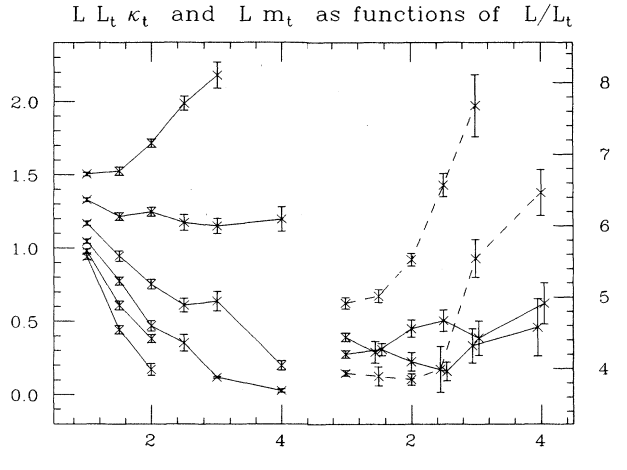

FIG. 12. Left-hand side: $L_t L\kappa_t$ as function of L ($L_t=4$) in the vicinity of the critical point. The connecting lines are to guide the eyes. Right-hand side: Lm_t as function of L ($L_t=4$) in the vicinity of the critical point, the dashed lines correspond to $\beta=2.28$, 2.34 and the solid lines to $\beta=2.30$, 2.32.

We conclude the section with remarks on string formation, which is the heart of almost all confinement scenarios. As other assumptions about the nonperturbative behavior of non-Abelian gauge theories, string formation has not been proven. However, it is generally believed to hold and also some numerical evidence has been reported.[79] For higher units of 't Hooft electric flux string formation predicts the relation (see Sec. 7.3 of Ref. 16)

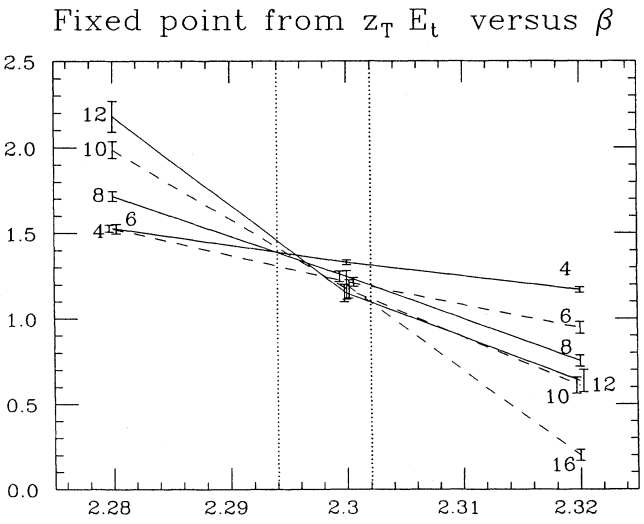

FIG. 13. Plot of LE_t vs β for $L=4$, 6, 8, 10, 12, and 16. To guide the eyes, results with $L=$const are connected by straight lines. (To increase the resolution some data points are slightly shifted in β.) Clearly, the indication is that the fixed point develops in the range $2.294 \leq \beta_c \leq 2.302$, as indicated by the dotted vertical lines.

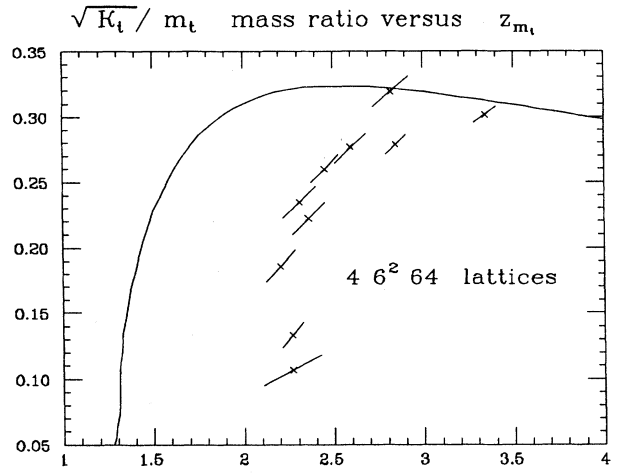

FIG. 14. Plot of $\sqrt{\kappa_t}/m_t$ vs z_{m_t} for $4\times6^2 64$ lattices. The solid line is an analytical result from Ref. 8 (in preparation).

$$E_n=\sqrt{n}E_1 \quad (n=1,2,\ldots)\,. \tag{3.10a}$$

In contrast, the adiabatic approximation[6,7] predicts

$$E_n \approx nE_1 \tag{3.10b}$$

for SU(2) (i.e., $n=1,2$) in the intermediate volume range. Figure 16, reproduced from Ref. 26, compares ratios for different units of electric flux with this prediction. The variable z_{E_1} (2.35b) is used. The results rely on the "supplementary" statistics of Table I and a table of the mass estimates is given in Ref. 26. From Fig. 16 it is obvious that there is very good agreement between MC results and the analytical prediction (3.10b) up to $z_{E_1}\approx 1$. For

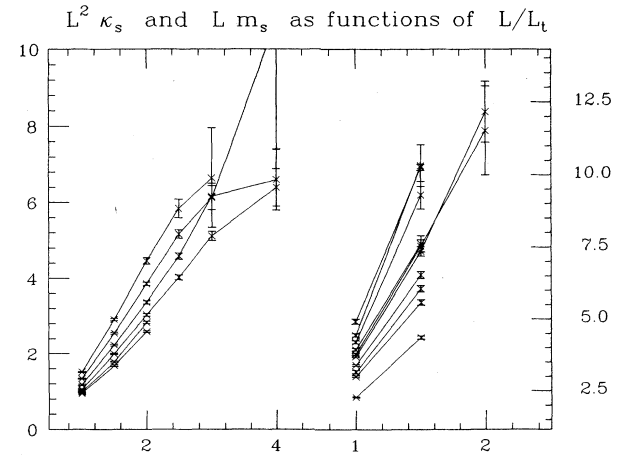

FIG. 15. Left-hand side: $L^2\kappa_s$ as function of L ($L_t=4$) in the vicinity of the critical point. Right-hand side: Lm_s as function of L ($L_t=4$) in the vicinity of the critical point.

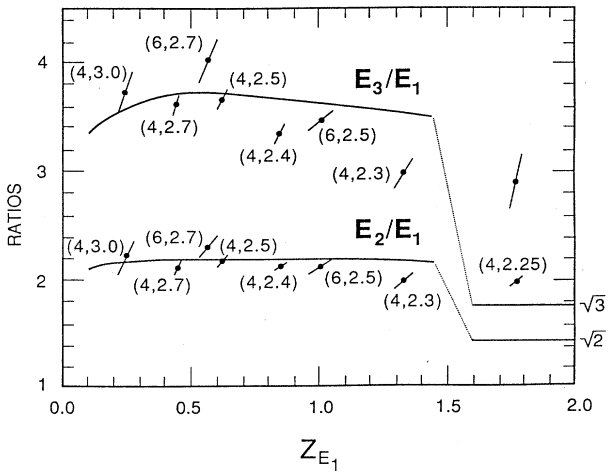

FIG. 16. MC results for E_3/E_1 and E_2/E_1 are plotted vs z_{E_1} (2.35b) and compared with the analytical predictions of Refs. 6 and 7. Data points are labeled by (L,β). The lines on the right-hand side indicate the asymptotic values expected (Ref. 16) from string formation.

larger z_{E_1} values the MC data lie slightly below the analytical curves, but this may well be explained by higher-order corrections to the analytical calculation and/or by inaccuracies of the somewhat limited data set.

In conclusion, in the investigated volume range we have no string formation. However, it would be premature to conjecture that such a mechanism does not take place at all. Instead, it is expected to occur at larger z_{E_1} values. Unfortunately, they are not directly accessible with our present simulation method. If it is true, that string formation sets in at values $z_{E_1} > 1.5$, then there is an amazingly large gap between the tunneling transition (at $z_{E_1} < 0.1$ the first relict of the deconfining phase transition on $L^3\infty$ lattices) and string formation, possibly the last relict of the deconfining phase transition on $L^3\infty$ lattices. Obviously instantons do not play any role for the tunneling transition, whereas they may well become important for the physics beyond $z_{E_1} \approx 1.5$ ($z_2 \approx 5$).

IV. SUMMARY AND CONCLUSIONS

We have carried out a detailed numerical investigation of SU(2) lattice gauge theory in medium-sized volumes. The results supplement (or are supplemented by) recent progress of analytical, continuum calculations in such volumes.[6-8] For $L^3\infty$ lattices it is natural to divide volumes into small, intermediate, and large. "Small" volumes are those before the tunneling transition, where $\sqrt{\kappa}/m(A_1^+) \approx 0$ holds. After the tunneling transition we have $\sqrt{\kappa}/m(A_1^+) = \mathcal{O}(1)$. More precisely, for this ratio we are close to the infinite-volume estimate $\sqrt{\kappa}/m(A_1^+) = 0.315(30)$ given by Eq. (3.5). However, there is no string formation yet. This defines the intermediate volume range. String formation is conjectured to set in when we proceed from intermediate to large volumes. As discussed in Sec. III E we were not able to find positive evidence within the limitations of our methods. (There is some support from other investigations.[79,83]) In the same volume range, where we expect string formation, the $m(E^+)$ mass is supposed to increase as indicated by Eqs. (3.4a) and (3.4b). In contrast, the mass ratios $\sqrt{\kappa}/m(A_1^+)$ and $m(T_2^+)/m(A_1^+)$ seem to stay relatively stable and we do not know what physical reason makes the $m(E^+)$ mass so special. A byproduct of our simulations is a precise determination of the $\Delta\beta(\beta)$ function, see Figs. 7(a) and 7(b).

Striking is the overall very satisfactory agreement of numerical and analytical results, see Figs. 9 and 11 and also Eq. (3.9b) vs Ref. 8. In view of the fact that most of the numerical work is done on rather small sized lattices, that the analytical calculations suffer from higher-order perturbative corrections and, worse, all kinds of not understood systematic corrections, this is rather surprising and gives rise to some optimism. It is desirable to extend not only the numerical[9] but also the analytical calculations to the SU(3) gauge group.

Note added in proof. Recently van Baal[84] informed us about minor errors in Refs. 6 and 7 which lead to maximal 3% correction for the analytical curves depicted in our Figs. 5, 9, 10, and 11. Of course, this would be hardly visible on the scale of our figures.

ACKNOWLEDGMENTS

We would like to thank Claus Vohwinkel for numerous useful discussions and for valuable collaboration on part of this work. This research project was partially funded by the Department of Energy under Contracts Nos. DE-FG05-87ER40319 and DE-FC05-85ER2500. It also received support from the Florida State University through use of its Cyber 205 and by its COFRS program.

APPENDIX A

We prove Eq. (2.18a), $a_0 \geq 0$. Let us define the scalar product

$$(c,b) = \sum_n c_n^n b_n^n e^{-m_n L_z} .$$

Note that $(1,1) = Z$; Schwarz inequality gives $(c,c)(1,1) \geq (1,c)^2$ or

$$Z \sum_n (c_n^n)^2 e^{-m_n L_z} \geq \left[\sum_n c_n^n e^{-m_n L_z} \right]^2 .$$

APPENDIX B

We comment on problems with the congruential random-number generator. Previously, other authors reported similar problems.[80] The results of this appendix emerged from a consistency check on our string-tension results. We estimate κ from the finite-size behavior of the "energy" E, defined as the average plaquette expectation value. (The usual internal energy is $1-E$.) This approach should be compared with Michael.[40] Our $E = E(L_z)$ data are fitted with the expression

TABLE X. Energy values. Average plaquette expectation value "energies" for 4^3L_z lattices at $\beta=3.0$ [full SU(2) group]. The numeration of data is identical with Table I. If not marked otherwise, a vectorized version of CDC's (see Cyber 205 FORTRAN manual) congruential random number generator is used. "Improved random numbers are congruential random numbers where at each call one (or a few) extra random numbers are generated but not used, see Ref. 64, for an explicit listing of the related computer code. One data set of this table relies on a shift register random number generator (Ref. 81).

No.	L_z	Energy	
06	16	0.723 592(8)	
07	16	0.723 591(6)	Hot start
08	16	0.723 603(8)	Improved random numbers
09	24	0.723 513(12)	
10	32	0.723 494(9)	
11	32	0.723 502(9)	Improved random numbers
12	64	0.723 380(8)	
13	64	0.723 386(8)	
14	64	0.723 380(12)	Hot start
15	64	0.723 426(8)	Improved random numbers
16	64	0.723 441(9)	Shift reg random numbers
17	128	0.723 451(5)	
18	128	0.723 458(7)	Hot start
19	128	0.723 419(6)	Improved random numbers

$$E(L_z)=\frac{e_0+e_1e^{-L_zL\kappa}}{1+e^{-L_zL\kappa}} . \tag{B1}$$

The formula for $E(L_z)$ would be (2.29) if we were talking about the mean spacelike plaquette. However we have kept the mean plaquette (spacelike and timelike together). Let $\mathcal{E}_{ss}$ denote the operator corresponding to E_{ss}. For the spacelike plaquette we have

$$E_{ss}=\frac{1}{Z}\mathrm{Tr}(\mathcal{E}_{ss}\mathcal{T}^{L_z}) \quad \text{with} \quad Z=\mathrm{Tr}(\mathcal{T}^{L_z}) .$$

Inserting a complete set of eigenstates of the transfer matrix it becomes

$$E_{ss}=\frac{1}{Z}\sum_n \langle n|\mathcal{E}_{ss}|n\rangle e^{-E_nL_z}$$

$$=\langle 0|\mathcal{E}_{ss}|0\rangle+\langle 1|\mathcal{E}_{ss}|1\rangle e^{-E_1L_z}+\cdots .$$

The axial gauge is implicit and the sum is over zero-charge states only. For timelike energy E_{st}, one obtains

$$E_{\mathrm{st}}=\frac{1}{Z}\mathrm{Tr}(\mathcal{U}\mathcal{T}\mathcal{U}\mathcal{T}^{L_z-1})$$

$$=\frac{1}{Z}\sum_{n,m}|\langle n|\mathcal{U}|m\rangle|^2e^{-E_m}e^{-E_n(L_z-1)} .$$

For $L_z\to\infty$ this has the behavior $E_{st}=(A+Be^{-E_1L_z})/Z$ with the same Z and E_1 as for E_{ss}. In conclusion we have Eq. (B1). There is however a problem with nonzero momentum states. E_{ss}, E_{st}, and Z receive contributions from states with all possible momenta, nevertheless one expects that L_z is large enough for formula (B1) to hold. In particular, in our application the lowest nonzero momentum is very high.

Our data for the internal energy $[E(L_z)]$ of 4^3L_z lattices at $\beta=3.0$ with the full group are given in Table X. Results using the usual congruential random-number generator present a minimum (around $L_z=64$), in contradiction with Eq. (B1). Sequences of numbers produced by this generator are known to exhibit strong autocorrelations at distances which are large power of 2. We believe that our results on 4^364 and 4^3128 lattices are affected by this problem. The estimated errors on the energies are stable with respect to the number of bins. We convinced ourselves that precision problems (like rounding errors) are not responsible for the discrepancies. The problem disappeared when, each time a vector of successive random numbers was computed, one or a few extra random numbers were also computed and not used. This avoids powers and even multiples of two. The problem also disappeared when shift-register random numbers[81] were used.

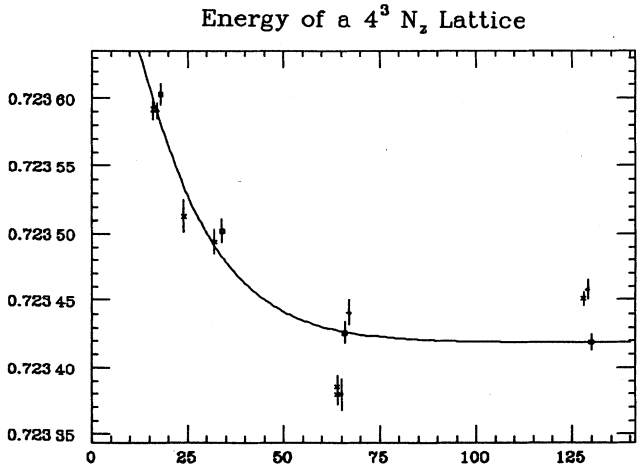

FIG. 17. Least-squares fit of our "energy" data according to Eq. (B1). Only data with improved and shift-register random numbers are included in the fit. The outcome is given by (B2a). For illustration the data (far off the fit line) spoiled by a bad choice of random numbers are also included in the figure.

A fit of the correct data with Eq. (B1) (for $L_z=16,24,32,64,128$) is depicted in Fig. 17 and gives

$$\sqrt{\kappa}=0.131(8),\quad e_0=0.723\,419(6)\,,$$
$$e_1=0.724\,14(8),\quad \chi^2=5.2\,. \tag{B2a}$$

Omitting the point $L_z=24$, which used the old random numbers (24 is however not a power of two) one obtains

$$\sqrt{\kappa}=0.127(7),\quad e_0=0.723\,417(6)\,,$$
$$e_1=0.724\,11(7),\quad \chi^2=0.3\,. \tag{B2b}$$

Both results are compatible with the preciser direct estimates 16–19 of Table III (a). Strange is the near equality of the constants e_0 and e_1. We are very close to a cancellation of the L_z dependence of numerator and denominator in the expression (B1) for $E(L_z)$.

*Present and permanent address: Service de Physique Théorique, CEN Saclay, F-91191 Gif-sur-Yvette, France.

[1]M. E. Fisher, in *Critical Phenomena,* proceedings of the 51st Enrico Fermi Summer School, Varena, edited by M. S. Green (Academic, New York, 1972).
[2]M. N. Barber, in *Phase Transitions and Critical Phenomena,* edited by C. Domb and J. L. Lebowitz (Academic, London, 1983), Vol. 8.
[3]E. Brezin, J. Phys. (Paris) **43**, 15 (1982); Ann. N.Y. Acad. Sci. **77**, 338 (1983).
[4]B. Berg and A. Billoire, Phys. Lett. **166B**, 203 (1986); Phys. Lett. B **185**, 446(E) (1987).
[6]B. Berg, A. Billoire, and C. Vohwinkel, Phys. Rev. Lett. **57**, 400 (1986).
[6]J. Koller and P. van Baal, Phys. Rev. Lett. **58**, 2511 (1987).
[7]J. Koller and P. van Baal, Nucl. Phys. **B302**, 1 (1988).
[8]B. Berg, C. Vohwinkel, and C. P. Korthals-Altes, Phys. Lett. B **209**, 319 (1988), and work in preparation.
[9]C. Vohwinkel and B. Berg, following paper, Phys. Rev. D **40**, 584 (1989).
[10]M. Lüscher, in *Progress in Gauge Field Theory,* proceedings of the Cargèse Summer Institute, Cargèse, France, 1983, edited by G. 't Hooft, A. Singer, and R. Stora (NATO Advanced Study Institute, Series B: Physics, Vol. 115) (Plenum, New York, 1984); Commun. Math. Phys. **104**, 177 (1986).
[11]A. Billoire, K. Decker, and R. Henzi, Phys. Lett. B **211**, 124 (1988).
[12]B. Berg, A. Billoire, and C. Rebbi, Ann. Phys. (N.Y.) **142**, 184 (1982); **146**, 470 (1983).
[13]B. Berg, A. Billoire, S. Meyer, and C. Panagiotakopoulos, Commun. Math. Phys. **97**, 31 (1985).
[14]T. DeGrand and C. Peterson, Phys. Rev. D **34**, 3180 (1986).
[15]C. Michael and M. Teper, Nucl. Phys. **B305** [FS23], 453 (1988).
[16]G. 't Hooft, Nucl. Phys. **B153**, 141 (1979).
[17]G. Mack and V. B. Petkova, Ann. Phys. (N.Y.) **125**, 117 (1980).
[18]J. Groenfeld, J. Jurkiewicz, and C. P. Korthals-Altes, Phys. Scr. **23**, 1022 (1981); Acta Phys. Pol. **B12**, 615 (1981).
[19]A. Gonzales-Arroyo, J. Jurkiewicz, and C. P. Korthals-Altes, in *Structural Elements in Particle Physics and Statistical Mechanics,* proceedings of the NATO Advanced Summer Institute on Theoretical Physics, Freiburg, West Germany, 1981, edited by J. Honerkamp, J. Pohlmeyer, and H. Römer (NATO ASI, Series B: Physics, Vol. 82) (Plenum, New York, 1983), p. 339.
[20]M. Lüscher, Nucl. Phys. **B219**, 233 (1983).
[21]M. Lüscher and G. Münster, Nucl. Phys. **B232**, 445 (1984).
[22]P. Weisz and V. Ziemann, Nucl. Phys. **B284**, 157 (1987).
[23]P. van Baal, Nucl. Phys. **B264**, 548 (1986); K. Koller and P. van Baal, *ibid.* **B273**, 387 (1986); Ann. Phys. (N.Y.) **174**, 299 (1987).
[24]B. Berg, in *Lattice Gauge Theory 86,* proceedings of the NATO ARW Workshop, Upton, New York, 1986, edited by H. Satz, I. Harrity, and J. Potvin (Plenum, New York, 1987).
[25]C. Vohwinkel, Phys. Lett. B **213**, 54 (1988).
[26]B. Berg, Phys. Lett. B **206**, 97 (1988).
[27]See, for instance, M. Creutz, *Quarks and Gluons on a Lattice* (Cambridge University Press, Cambridge, England, 1983); A. Hasenfratz and P. Hasenfratz, Annu. Rev. Nucl. Part. Sci. **35**, 559 (1985); C. Rebbi, *Lattice Gauge Theory and Monte Carlo Simulations,* edited by C. Rebbi (World Scientific, Singapore, 1983).
[28]K. G. Wilson, Phys. Rev. D **10**, 2445 (1974).
[29]W. E. Caswell, Phys. Rev. Lett. **33**, 244 (1974); D. R. T. Jones, Nucl. Phys. **B75**, 531 (1974).
[30]K. Symanzik, Nucl. Phys. **B226**, 187 (1983); **B226**, 205 (1983).
[31]A. M. Polyakov, Phys. Lett. **72B**, 477 (1978); L. Susskind, Phys. Rev. D **20**, 2610 (1979).
[32]L. D. McLerran and B. Svetitsky, Phys. Lett. **98B**, 195 (1981); Phys. Rev. D **24**, 450 (1981); J. Kuti, J. Polonyi, and K. Szlachanyi, Phys. Lett. **98B**, 199 (1981); J. Engels, F. Karsch, I. Montvay, and H. Satz, Nucl. Phys. **B205** [FS6], 545 (1982).
[33]A. Hasenfratz and P. Hasenfratz, Nucl. Phys. **B193**, 210 (1981), and references therein.
[34]M. Creutz, Phys. Rev. D **15**, 1128 (1977); M. Lüscher, Commun. Math. Phys. **54**, 283 (1977).
[35]See, for instance, M. Reed and B. Simon, *Methods of Modern Mathematical Physics* (Academic, New York, 1978), Vols. 1 and 4.
[36]H. Fritzsch and P. Minkowski, Nuovo Cimento **30A**, 393 (1975), and references given therein.
[37]C. Borgs and E. Seiler, Commun. Math. Phys. **91**, 329 (1983).
[38]M. Lüscher, K. Symanzik, and P. Weisz, Nucl. Phys. **B173**, 365 (1980); about the possibility of other universality classes, see P. Olesen, Phys. Lett. **160B**, 144 (1985).
[39]G. Münster, Nucl. Phys. **B180** [FS2], 23 (1981).
[40]C. Michael, J. Phys. G **13**, 1001 (1987).
[41]H. Bethe, Ann. Phys. (Leipzig) **3**, 133 (1929).
[42]J. Kogut, D. K. Sinclair, and L. Susskind, Nucl. Phys. **B114**, 199 (1976).
[43]B. Berg and A. Billoire, Nucl. Phys. **B221**, 109 (1983); **B226**, 405 (1983).
[44]B. Berg, in *Progress in Gauge Field Theory* (Ref. 10).
[45]G. Parisi, R. Petronzio, and F. Rapuano, Phys. Lett. **128B**, 418 (1983).
[46]C. Bernard, Phys. Lett. **108B**, 431 (1982); Nucl. Phys. **B219**, 341 (1983); J. Ambjorn, P. Olesen, and C. Peterson, *ibid.* **B240** [FS12], 189 (1984); C. Michael, *ibid.* **B259**, 58 (1985).
[47]A. Billoire and E. Marinari, Phys. Lett. **139B**, 399 (1984).

[48]H.-Q. Ding, Phys. Lett. B **200**, 133 (1988).
[49]R. L. Dobrushin, Theory Probab. Its Appl. (USSR) **13**, 197 (1969); O. E. Lanford III and D. Ruelle, Commun. Math. Phys. **13**, 194 (1969).
[50]M. Abramowitz and I. Stegun, *Handbook of Mathematical Functions* (Dover, New York, 1968).
[51]B. Berg, A. Billoire, and C. Vohwinkel, Phys. Lett. B **191**, 157 (1987).
[52]B. Berg, A. Billoire, and R. Salvador, Phys. Rev. D **37**, 3774 (1988).
[53]Ph. de Forcrand, G. Schierholz, H. Schneider, and M. Teper, Phys. Lett. **160B**, 137 (1985).
[54]F. Gutbrod, Phys. Lett. B **186**, 389 (1987).
[55]E. Brezin and J. Zinn-Justin, Nucl. Phys. **B257** [FS14], 867 (1985).
[56]I. Bender, B. Berg, and W. Wetzel, Nucl. Phys. **B269**, 389 (1986).
[57]A. Hasenfratz and P. Hasenfratz (Ref. 27).
[58]S. Brandt, *Statistical and Computational Methods in Data Analysis* (North-Holland, Amsterdam, 1970).
[59]B. L. van der Waerden, *Mathematical Statistics* (Springer, Berlin, 1969); W. S. Gosset, Biometrika **6**, 1 (1908).
[60]B. Efron, SIAM Rev. **21**, 460 (1979), and references therein.
[61]S. Gottlieb, P. B. Mackenzie, H. B. Thacker, and D. Weingarten, Nucl. Phys. **B263**, 704 (1986); R. Gupta, G. Guralnik, G. Kilcup, A. Patel, S. Sharpe, and T. Warnock, Phys. Rev. D **36**, 2813 (1987).
[62]G. Bhanot, C. Lang, and C. Rebbi, Comput. Phys. Commun. **25**, 275 (1982).
[63]M. Creutz and G. Bhanot, Phys. Rev. D **24**, 3212 (1981).
[64]C. Vohwinkel, B. Berg, and A. Devoto, Comput. Phys. Commun. **51**, 331 (1988).
[65]C. Rebbi, Phys. Rev. D **21**, 3350 (1980); D. Petcher and D. H. Weingarten, *ibid.* **22**, 2465 (1980).
[66]G. Mack and E. Pietarinen, Phys. Lett. **94B**, 397 (1980).
[67]A. Patel and R. Gupta, Nucl. Phys. **B251** [FS13], 789 (1985).
[68]U. Heller and F. Karsch, Phys. Rev. Lett. **54**, 1765 (1985).
[69]R. Sommer, Nucl. Phys. **B306**, 181 (1988).
[70]F. Gutbrod, Z. Phys. C **37**, 143 (1987).
[71]I. Muzinich and V. Nair, Phys. Lett. B **178**, 105 (1986).
[72]C. Michael, M. Teper, and G. Tickle, Phys. Lett. B **207**, 313 (1988).
[73]G. Münster, Nucl. Phys. **B190** [FS3], 439 (1981); **B205** [FS5], 648(E) (1982).
[74]G. Curci and R. Tripiccione, Phys. Lett. **151B**, 145 (1985).
[75]J. Engels, J. Jersák, K. Kanaya, E. Laermann, C. B. Lang, T. Neuhaus, and H. Satz, Nucl. Phys. **B280** [FS18], 577 (1987).
[76]See, for instance, Kerson Huang, *Statistical Mechanics* (Wiley, New York, 1987).
[77]E. Manousakis and J. Polonyi, Phys. Rev. Lett. **58**, 847 (1987).
[78]E. D'Hoker, Nucl. Phys. **B180**, 341 (1981); J. Karliner and G. Mack, *ibid.* **B225** [FS9], 371 (1983), and references therein.
[79]J. Wosiek, Nucl. Phys. B (Proc. Suppl.) **4**, 52 (1988), and references given therein.
[80]G. Kalle and S. Wansleben, Comput. Phys. Commun. **33**, 343 (1984); K. Jansen, J. Jersák, and T. Neuhaus, *Proceedings of the 1984 Conference on Cyber 200, Bochum,* edited by H. Ehlich (Bochum University Press, Bochum, 1985); T. Filk, K. Fredenhagen, and M. Marcu, Phys. Lett. **165B**, 125 (1985).
[81]S. Wansleben, J. G. Zabolitzky, and G. Kalle, J. Stat. Phys. **32**, 271 (1984).
[82]S. A. Chin, C. Long, and D. Robson, Phys. Rev. Lett. **60**, 1467 (1987).
[83]A. Hasenfratz, P. Hasenfratz, and F. Niedermayer, Bern Report No. BUTP-01/89, 1989 (unpublished).
[84]Pierre van Baal, CERN Report No. TH-5359/89, 1989 (unpublished).